

Identification of ca. 850 Ma high-temperature strongly peraluminous granitoids in southeastern Guizhou Province, South China: A result of early extension along the southern margin of the Yangtze Block



Tao Wu^a, Jia-Xi Zhou^{b,*}, Xuan-Ce Wang^{c,d}, Wu-Xian Li^e, Simon A. Wilde^c, Hai-Rui Sun^f, Jing-Song Wang^g, Zhen Li^c

^a School of Earth Sciences, Zhejiang University, Hangzhou 310027, China

^b State Key Laboratory of Ore Deposit Geochemistry, Institute of Geochemistry, Chinese Academy of Sciences, Guiyang 550081, China

^c The Institute for Geoscience Research, Department of Applied Geology, Curtin University, GPO Box U1987, Perth, WA 6845, Australia

^d School of Earth Science and Resources, Chang'an University, Shaanxi, Xi'an 710054, China

^e State Key Laboratory of Isotope Geochemistry, Guangzhou Institute of Geochemistry, Chinese Academy of Science, Guangzhou 510640, China

^f Development Research Center of China Geological Survey, Beijing 100037, China

^g The 102 Geological Team, Guizhou Bureau of Exploration and Development of Geology and Mineral Resources, Zunyi 563003, China

ARTICLE INFO

Keywords:

Early Neoproterozoic
Strongly peraluminous granitoids
Anorogenic magmatism
South China

ABSTRACT

Strongly peraluminous granites are characterized by high A/CNK values (> 1.1) and are important for understanding the regional tectonic regime. Here, we present integrated studies of zircon U-Pb ages, trace elements and Lu-Hf isotopes, whole-rock major and trace elements, and Nd isotope compositions for the newly discovered Nage granite porphyry in southeastern Guizhou Province. The porphyry has a crystallization age of 852 ± 5 Ma and shows wide ranges in SiO₂ (64.5–72.51 wt%) and Al₂O₃ (13.08–19.34 wt%) contents, with low TiO₂ (0.41–0.84 wt%) and P₂O₅ (< 0.15 wt%) contents. All the samples are strongly peraluminous with A/CNK > 1.1, and they have similar trace element patterns with depletion in high field strength elements (HFSE, e.g., Nb and Ta) and enrichment in large-ion lithophile elements (LILE, e.g., Rb, Th and U). Initial zircon Hf isotopes of the porphyry vary from ε_{Hf(t)} = -7.6 to -0.6, whereas whole-rock Nd isotopes are relatively uniform with ε_{Nd(t)} = -6.0 to -6.7. They record high zircon saturation temperatures (T_{zr}) (786–842 °C, mostly > 810 °C), but low oxygen fugacity (log fO₂ = -16 to -25, corresponding to ΔFMQ -3 to ΔFMQ -7) and emplacement pressure of < 0.5 GPa. Major and trace elements, 10,000 Ga/Al ratios and Zr + Nb + Ce + Y values, show good correlations with T_{zr}, indicating that fractional crystallization may have played an important role. Although these granites show low P₂O₅ contents that decrease with increasing Rb, the high A/CNK (> 1.1), K₂O/Na₂O (0.7–2.6; average 1.4) and CaO/Na₂O (0.2–0.8; mostly > 0.5) ratios suggest that clay-poor metasedimentary rock were dominant in the source. Combined with the Nd-Hf isotopes, we suggest that the Nage granite porphyry formed by anatexis of an immature arkose and greywacke source, which was a mixture of weathered juvenile igneous materials and minor recycled ancient crustal components. The ca. 850 Ma strongly peraluminous granites, along with coeval extension-related magmatism along the southwestern margin of the Yangtze Block, indicate an extensional environment started as early as ca. 850 Ma.

1. Introduction

Strongly peraluminous granitoids are characterized by high A/CNK values (molar ratio of Al₂O₃/(CaO + Na₂O + K₂O) > 1.1) and are crucial for constraining the regional tectonic history (e.g., Sylvester, 1998; Clemens, 2003; Zhao et al., 2013a; Chappell et al., 2012; Wang et al., 2013; Peng et al., 2015). However, their petrogenesis still

remains controversial. For example, their high A/CNK ratios can be derived by fractionation of amphibole and pyroxene, contamination by surrounding sedimentary rocks, or by loss of alkalis through later weathering and alteration (e.g., Zen, 1988; Wu et al., 2017a). Previous study suggested that even partial melting of igneous rocks can also generate granitic melts with A/CNK > 1.1 (e.g., Patiño Douce, 1999). Therefore, identification of strongly peraluminous granitoids in ancient

* Corresponding author at: State Key Laboratory of Ore Deposit Geochemistry, Institute of Geochemistry, Chinese Academy of Sciences, No. 99 West Lincheng Road, Guiyang 550081, China.

E-mail address: zhoujiaxi@vip.gyig.ac.cn (J.-X. Zhou).

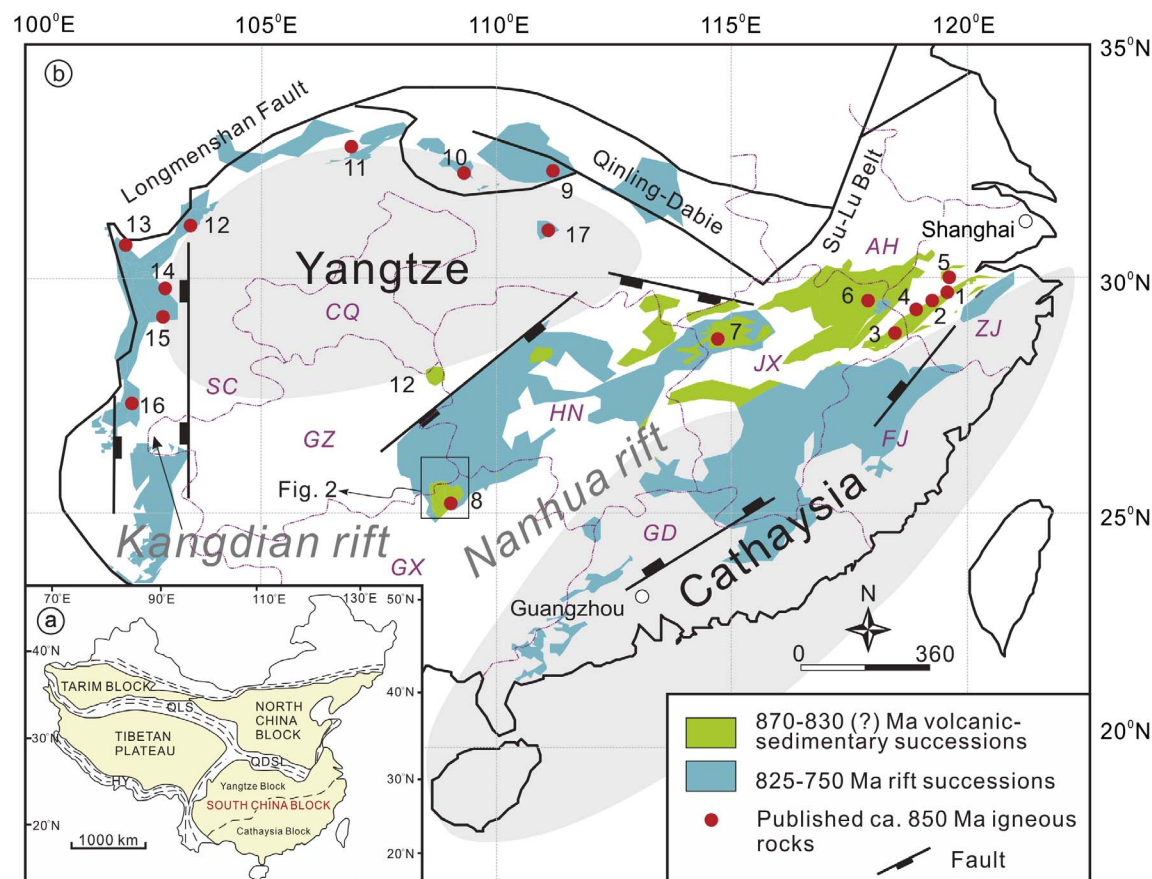


Fig. 1. (a) Geotectonic map of China showing the location of major tectonic units (modified after Li et al., 2010a,b). (b) Simplified regional geological map of South China. QLS: Qilianshan fold belt, QDSL: Qinlin-Dabie-Su-Lu orogenic belt, HY: Himalaya fold belt. ZJ-Zhejiang Province; AH-Anhui Province; JX-Jiangxi Province; HN-Hunan Province; GX-Guangxi Province; FJ-Fujian Province; GD-Guangdong Province; CQ-Chongqing city; SC-Sichuan Province. Data sources for the ca. 850 Ma igneous rocks are: 1. 838 ± 5 Ma Chencai bimodal volcanic rocks and 841 ± 6 Ma Lipu diorite (Li et al., 2010a,b); 2. 849 ± 7 Ma Shenwu doleritic dyke (Li et al., 2008a,b,c); 3. 848 ± 4 Ma Gangbiyan alkaline complex (Li et al., 2010a,b); 4. 842 ± 5 Ma Jiangshan Pluton (Liu et al., 2015); 5. $845-847$ Ma Shanhou Pluton (Liu et al., 2015); 6. 849 ± 6 Ma Zhenzhushan bimodal volcanic rocks (Li et al., 2010a,b); 7. 847 ± 18 Ma Fanxian dolerite (Zhang et al., 2013); 8. 855 ± 5 Ma Yuambaoshan gabbro (Yao et al., 2014); 9. ca. 860 Ma Sanligang granitoids (Xu et al., 2016); 10. 844 ± 2 Ma Fangcheng syenite (Bao et al., 2008); 11. 860 ± 5 Ma K-rich Shuimo syenites (Gan et al., 2016); 12. 848 ± 4 Ma Baoxing gabbro (Meng et al., 2015); 13. 864 ± 8 Ma Gezong granite (Zhou et al., 2002); 14. 851 ± 15 Ma Tianquan granite (Lai et al., 2015); 15. 853 ± 42 Ma Lugouqiao gabbro (Shen et al., 2002); 16. ca. 860 Ma Guangdaoshan dioritic-gabbroic pluton (Du et al., 2014); and 17. 850 Ma Huangling tonalite and trondhjemite (Zhao et al., 2013b).

orogenic belts can shed new light on the tectonic history of the orogenic belt.

The South China Block (SCB) is composed of the Yangtze Block to the northwest and the Cathaysia Block to the southeast (Fig. 1a). It is widely accepted that the Yangtze and Cathaysia blocks amalgamated during the Proterozoic, but the timing and mechanism is hotly debated. One proposal is that amalgamation was related to the worldwide Grenvillian orogenic event associated with the assembly of Rodinia (e.g., Li et al., 1995, 2002, 2007, 2006, 2009, 2008a,b,c; Wang et al., 2007, 2008, 2009, 2010, 2011), whereas an alternative view is that the resultant orogenic event lasted until ca. 820 Ma or even longer (e.g., Zhao and Cawood, 1999, 2012; Zhou et al., 2002; Wu et al., 2006; Zheng et al., 2007; Zhao et al., 2011). Therefore, magmatism that was earlier than 820 Ma in the SCB is important for understanding the amalgamation history between the Yangtze and Cathaysia blocks. However, earlier studies have proposed a period of magmatic quiescence between ca. 900 and ca. 830 Ma in the Yangtze Block (e.g., Li et al., 2003a,b, 2006, 2008a,b,c). In recent years, more and more igneous rocks with ages of ca. 850 Ma have been recognized throughout the Yangtze Block (Fig. 1b). Geochronological studies of detrital zircons from Neoproterozoic sedimentary rocks of the Sibao and Lengjiaxi groups also show a pronounced age peak at 850–860 Ma (Yang et al., 2015; Wang et al., 2012a). This suggests an important magmatic event at ca. 850 Ma in the SCB, which will provide important constraints on the amalgamation history between the two blocks.

Although many ca. 850 mafic and felsic rocks have been reported in the southeastern Yangtze Block (Li et al., 2008a,b,c, 2010a,b; Liu et al., 2015; Lyu et al., 2017), a few igneous rocks have been recognized in the central and southwestern parts of the block (Zhang et al., 2013; Yao et al., 2014; Lin et al., 2016) (Fig. 1b). Recently, several granite porphyries were discovered in drill holes at Nage, in the southwestern Yangtze Block (Fig. 2a). In this contribution, we carried out integrated studies of zircon U-Pb geochronology, trace element and Lu-Hf isotopes, whole-rock geochemistry and Nd isotopes on the Nage granite porphyry. When combined with previous data, we propose that juvenile igneous materials have been incorporated into the source of these granitoids and that extensive extension/rift activity along the southern margin of Yangtze Block, which may be related to the initial break-up of the Rodinia supercontinent, may have occurred at as early as ca. 850 Ma.

2. Geological background

The basement rocks of the Yangtze Block contain high-grade metamorphosed tonalite, trondhjemite and granodiorite gneisses (TTG) and amphibolites as old as 3.45 Ga (Qiu et al., 2000; Zheng et al., 2006; Liu et al., 2008; Guo et al., 2014), whereas those of the Cathaysia Block are composed of schist, gneiss, amphibolite, migmatite and meta-volcanic rocks formed during the Paleoproterozoic to Neoproterozoic (e.g., Yu et al., 2009, 2010; Liu et al., 2008). The recent identified

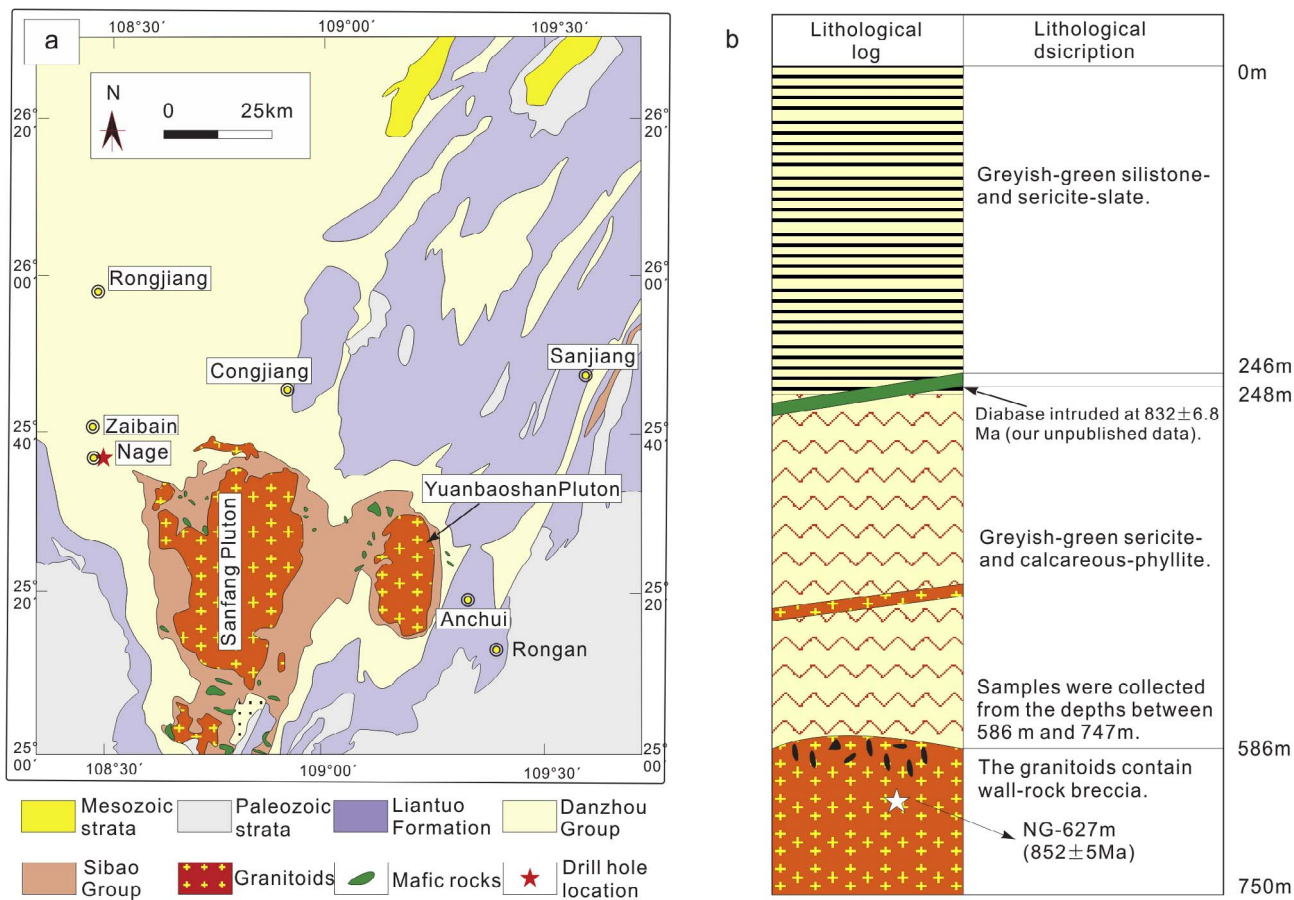


Fig. 2. (a) Simplified geological map of the Nage area (modified after Li, 1999) and (b) drill hole data log showing the location of the dated sample.

Hadean zircons grains may suggest the presence of much older basement in the Cathaysia Block (Xing et al., 2014).

Many Neoproterozoic igneous rocks are present in the southwestern Yangtze Block (Yao et al., 2014; Wang et al., 2013; Zhao et al., 2013a; Lin et al., 2016; Wang et al., 2007, 2009). Generally, they show a bimodal distribution. The mafic-ultramafic end-member consists of metabasalts, meta-basaltic andesite, gabbro, dolerite and olivine pyroxenite, with formation ages ranging from 860 Ma to 750 Ma (Zhou et al., 2009; Yao et al., 2014; Lin et al., 2016; Wang et al., 2007, 2009), whereas the felsic end-member consists of granitoids with crystallization ages ranging from 836 Ma to 794 Ma (Li et al., 2003; Wang et al., 2006, 2013; Zhao et al., 2013a). Granitic plutons are mainly exposed in northern Guizhou Province, including the Sanfang ($\sim 1000 \text{ km}^2$), Bendong ($\sim 40 \text{ km}^2$), Zhaigun ($\sim 11 \text{ km}^2$), Tianpeng ($\sim 10 \text{ km}^2$), and Fanjingshan plutons (composed mainly of small granitic stocks $< 1 \text{ km}^2$). They intruded into the Mesoproterozoic Sibao metamorphic basement, and were covered unconformably by the Neoproterozoic Danzhou sedimentary rocks (Li, 1999). Previous studies have demonstrated that these granitoids are all strongly peraluminous with $A/\text{CNK} > 1.1$ (Li, 1999; Li et al., 2003).

The Nage granite porphyry is located to the west of the Sanfang pluton ($108^\circ 29'E$; $25^\circ 35'N$; Fig. 2a) and was intersected in bore holes drilled for mineral exploration. These felsic rocks occur at $> 580 \text{ m}$ depth and their base is unconstrained (Fig. 2b). Several samples were collected from different depths ranging from 586 to 747 m (Fig. 2b). All the samples have porphyritic texture and show various degrees of alteration. They contain phenocrysts (30–40 vol%) composed mainly of quartz (25–30 vol%), plagioclase (5–10 vol%), K-feldspar ($\sim 5 \text{ vol\%}$) and biotite (5–10 vol%) (Fig. 3). Minor accessory minerals include zircon, apatite and monazite.

3. Analytical methods

Zircon grains were separated from granitic sample NG-627 using conventional heavy liquid and magnetic techniques, handpicked, mounted in epoxy resin and then polished to expose the grain centers. The samples were then carbon coated and cathodoluminescence (CL) images were taken to select sites for analysis. The U-Pb geochronology of zircon was conducted by LA-ICP-MS at the State Key Laboratory of Ore Deposit Geochemistry (SKLODG), Institute of Geochemistry, Chinese Academy of Sciences (IGCAS), Guangzhou. A GeoLasPro laser-ablation system (Lamda Physik, Gottingen, Germany) and an Agilent 7700x ICP-MS (Agilent Technologies, Tokyo, Japan) were combined for the experiments. The 193 nm ArF excimer laser, homogenized by a set of beam delivery systems, was focused on the zircon surface with a fluence of 10 J/cm^2 . According to the grain size of the zircon, the ablation protocol employed spot diameters of $44 \mu\text{m}$ at 3 or 5 Hz repetition rates for 40 s (equating to 120 and 200 pulses). Helium was used as the carrier gas to efficiently transport aerosols to the ICP-MS. Zircon 91,500 was used as an external standard to correct instrumental mass discrimination and elemental fractionation. Zircon GJ-1 and Plešovice were utilized as quality controls. The Pb abundance of zircon was externally calibrated against NIST SRM 610 using Si as an internal standard, whereas Zr was used as an internal standard for the other trace elements (Hu et al., 2011; Liu et al., 2010). The age calculations and concordia diagrams were made using the Isoplot/Ex v. 3.23 program (Ludwig, 2003). Trace element concentrations were calibrated by using ^{29}Si as an internal standard and NIST SRM 610 as an external standard. Uncertainties on individual and pooled analyses are reported at 1σ and 2σ level, respectively.

In situ zircon Hf isotope analyses were carried out using a Neptune Plus MC-ICP-MS (Thermo Fisher Scientific, Germany) in combination

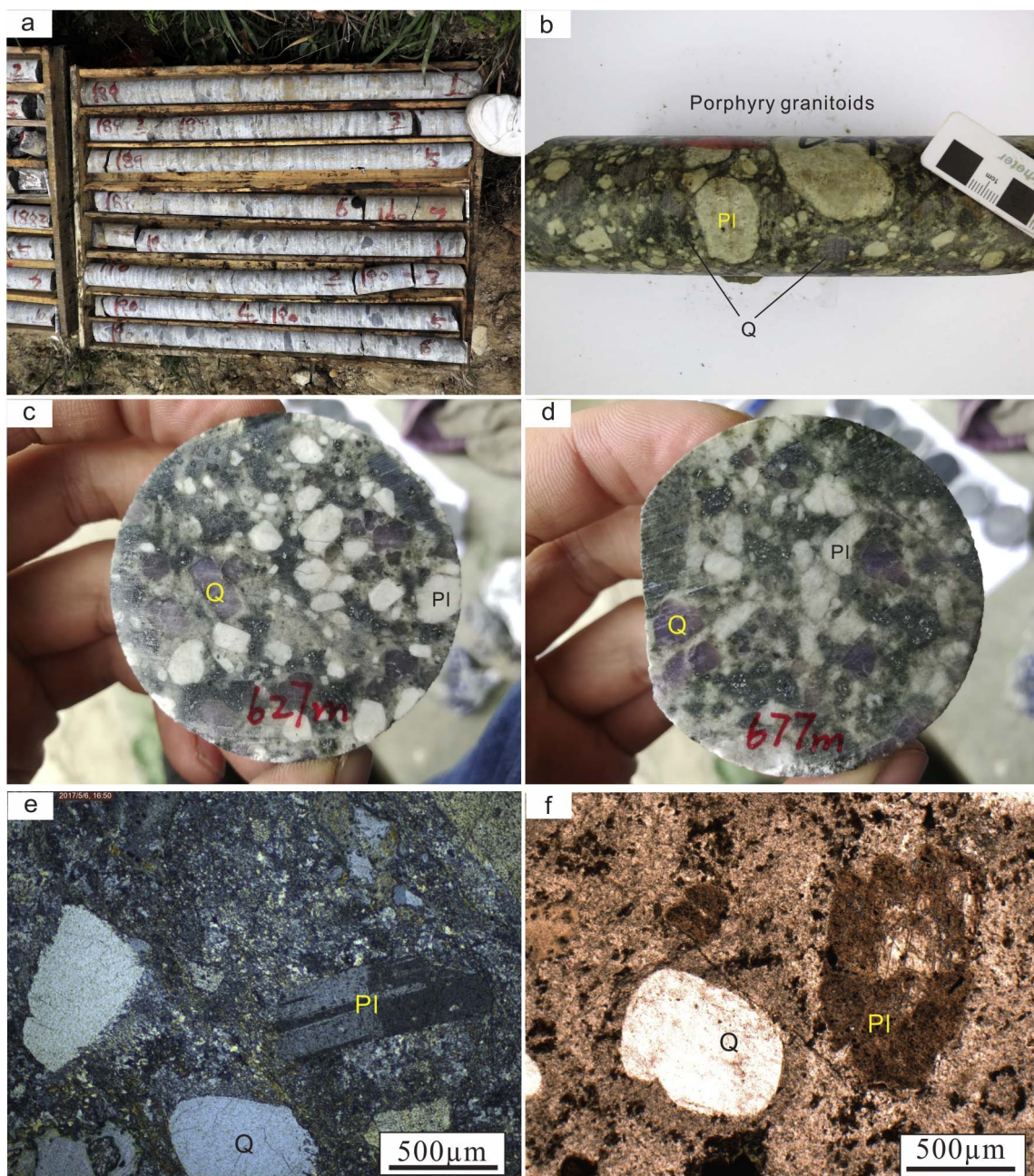


Fig. 3. Representative photographs and photomicrographs of samples from the Nage granite porphyry. (a) drill core of the Nage granite porphyry; (b) porphyric texture of the granitoids; (c) and (d) samples collected from 627 and 677 m depth, respectively; (e) and (f) mineral assemblages of the porphyry in relatively fresh (e) and altered samples (f). Note: Q, quartz; Pl, plagioclase.

with a Geolas 2005 excimer ArF laser ablation system (Lambda Physik, Göttingen, Germany) hosted at the State Key Laboratory of Geological Processes and Mineral Resources (GPMR), Wuhan. We selected the same CL domains for analysis as where used for U-Pb dating, guided by the CL images. Detailed operating conditions for the laser ablation system, MC-ICP-MS and analytical methods were the same as outlined by Hu et al. (2012).

Major oxides were analyzed by X-ray fluorescence spectrometry (XRF) at the SKLODG. The analytical errors for major oxides were generally within $\pm 5\%$. Trace element and rare earth element abundances were determined using a PE Elan 6000 ICP-MS at SKLODG. The powdered samples (50 mg) were dissolved in high-pressure Teflon bombs using a HF + HNO₃ mixture for 48 h at 190 °C (Qi et al., 2000). Rhenium was used as an internal standard to monitor signal drift during analysis. The Chinese National standards GSR-1 and GSR-3 and the

international standards GBPG-1 and OU-6 were used for analytical quality control. The analytical precision was generally within $\pm 10\%$ for most trace elements.

whole-rock Nd isotope measurements were conducted using thermal ionization mass spectrometry (TIMS) at the SKLODG. Samples were dissolved in HF + HClO₄. REE were separated using AGW50 \times 12 cation exchange columns. The REE were further dissolved in 0.1 N HCl, then Sm and Nd were separated using levextrel resin ion exchange columns. $^{147}\text{Sm}/^{144}\text{Nd}$ ratios were calculated using the Sm and Nd abundances measured by ICP-MS. The mean $^{143}\text{Nd}/^{144}\text{Nd}$ ratios for the La Jolla and Jndi-1 Nd standards were 0.511544 ± 3 (2σ) and 0.512104 ± 5 (2σ), respectively. $^{143}\text{Nd}/^{144}\text{Nd}$ ratios were normalized to the value of $^{146}\text{Nd}/^{144}\text{Nd} = 0.7219$.

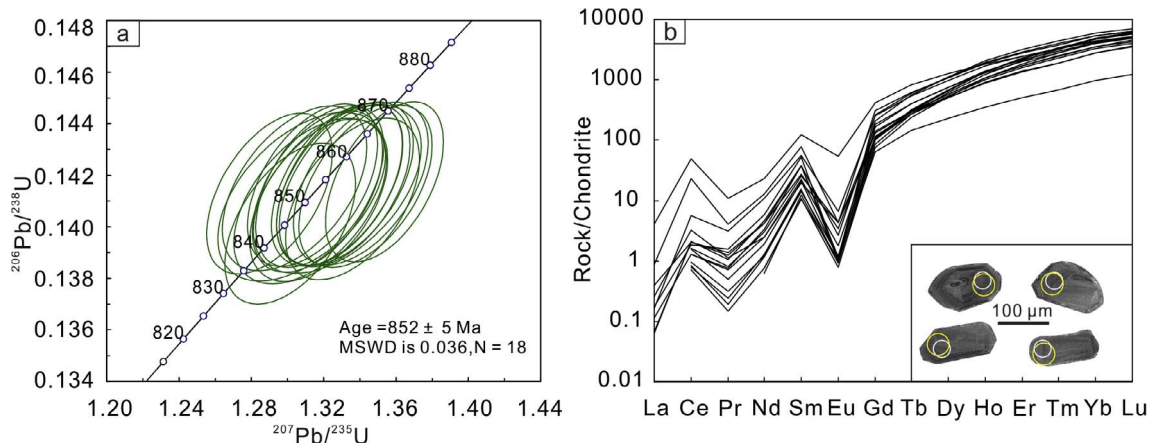


Fig. 4. (a) Zircon U–Pb concordia diagram of sample NG-627; (b) chondrite-normalized REE patterns of zircons from the Nage granite porphyry and representative cathodoluminescence (CL) images of zircons, with small and large circles showing areas of U–Pb and Lu–Hf isotope analysis, respectively. Chondrite-normalized values are from Sun and McDonough (1989).

4. Analytical results

4.1. Zircon U–Pb geochronology, trace elements and Lu–Hf isotopes

Zircon grains from sample NG-627 are euhedral to subhedral in crystal shape and are transparent and colorless, ranging from 90 to 150 μm in length, with length/width ratios varying from 1.5:1 to 3:1. Euhedral oscillatory zoning is common in most crystals in CL images (Fig. 4). Eighteen zircon crystals were dated (Table 1) and their Th/U ratios range from 0.1 to 1.4, reflecting a magmatic origin. They have $^{206}\text{Pb}/^{238}\text{U}$ ages ranging from 841 to 869 Ma and record a weighted mean age of 852 ± 5 Ma ($N = 18$, MSWD = 0.036; Fig. 4a).

Zircon trace element analyses were conducted simultaneously with zircon U–Pb analyses. They display enrichment in HREE, with negative Eu anomalies ($\text{Eu/Eu}^* = 0.01\text{--}0.24$; Fig. 4b and Table 2) and positive Ce anomalies (Fig. 4b). Zircon Lu–Hf isotopes were also analyzed on the same CL imaged zircon domains (Fig. 4b), and the results are listed in Table 3. They have a wide range of $^{176}\text{Lu}/^{177}\text{Hf}$ (0.000759–0.002673) and $^{176}\text{Hf}/^{177}\text{Hf}$ (0.282049–0.282255) ratios, with corresponding $\epsilon_{\text{Hf}}(t)$ values ranging from −7.5 to −0.6, and T_{DM2} model ages of 1.77–2.20 Ga.

4.2. Whole-rock geochemistry

The whole-rock major and trace element data are presented in Table 4. The fifteen porphyry samples have a wide range of SiO_2 (64.5–72.51 wt%), Al_2O_3 (13.08–19.34 wt%) and $\text{Na}_2\text{O} + \text{K}_2\text{O}$ (4.66–8.86 wt%) contents. They have low TiO_2 (0.41–0.84 wt%) and P_2O_5 (< 0.15 wt%) contents and are granite and granodiorite in composition with a strongly peraluminous affinity ($A/\text{CNK} = 1.1\text{--}2.5$; Fig. 5a, b).

In the primitive mantle-normalized spidergram (Fig. 6a), all the samples show similar trace element patterns, with depletion in high field strength elements (HFSE, e.g., Nb and Ta) and enrichment in large-ion lithophile elements (LILE, e.g., Rb, Th and U). They have negative Ba, Nb, Ta, and Eu anomalies, with exceptionally strong Sr depletion. They also show LREE enrichment patterns in the chondrite-normalized diagram, with $(\text{La/Yb})_N$ ratios ranging from 7 to 17, and have moderate negative Eu anomalies ($\text{Eu/Eu}^* = 0.4\text{--}0.6$; Fig. 6b).

Eight samples were also selected for whole-rock Nd isotope analysis. The results are listed in Table S1. In contrast to the zircon Lu–Hf isotopes, the samples have relatively uniform whole-rock Nd isotopes with a narrow range of $^{143}\text{Nd}/^{144}\text{Nd}$ ratios (0.511875–0.511899) and $\epsilon_{\text{Nd}}(t)$ values (−6.0 to −6.7).

Table 1

LA-ICP-MS zircon U–Pb ages of the Nage granite porphyry, southeastern Guizhou Province, South China.

Analysis_No.	Contents (ppm)		Th/U	$^{207}\text{Pb}/^{206}\text{Pb}$		$^{207}\text{Pb}/^{235}\text{U}$		$^{206}\text{Pb}/^{238}\text{U}$		$^{207}\text{Pb}/^{206}\text{Pb}$		$^{206}\text{Pb}/^{238}\text{U}$		$^{207}\text{Pb}/^{235}\text{U}$	
	Th	U		Ratios	1 σ	Ratio	1 σ	Ratio	1 σ	Age (Ma)	1 σ	Age (Ma)	1 σ	Age (Ma)	1 σ
NG-01	49	342	0.14	0.069	0.002	1.343	0.024	0.142	0.002	893	66	854	12	865	11
NG-02	123	249	0.49	0.068	0.002	1.327	0.024	0.142	0.002	867	66	854	12	858	10
NG-03	313	368	0.85	0.068	0.002	1.329	0.023	0.142	0.002	869	65	854	12	858	10
NG-04	89	372	0.24	0.067	0.002	1.314	0.024	0.142	0.002	846	66	854	12	852	10
NG-05	60	202	0.3	0.068	0.002	1.317	0.025	0.141	0.002	860	67	851	12	853	11
NG-06	58	206	0.28	0.067	0.002	1.304	0.026	0.141	0.002	832	69	853	12	847	12
NG-07	1222	891	1.37	0.069	0.002	1.354	0.022	0.142	0.002	906	63	855	12	869	9
NG-08	97	241	0.4	0.069	0.002	1.341	0.025	0.142	0.002	887	66	854	12	864	11
NG-09	107	295	0.36	0.068	0.002	1.328	0.031	0.141	0.002	870	72	853	12	858	13
NG-10	64	319	0.2	0.068	0.002	1.332	0.024	0.142	0.002	875	66	854	12	860	10
NG-11	37	322	0.11	0.068	0.002	1.317	0.024	0.141	0.002	854	66	852	12	853	10
NG-12	663	626	1.06	0.067	0.002	1.301	0.024	0.14	0.002	849	66	845	12	846	11
NG-13	58	125	0.46	0.067	0.002	1.308	0.031	0.141	0.002	843	73	851	12	849	13
NG-14	51	355	0.14	0.069	0.002	1.336	0.024	0.141	0.002	889	66	851	12	862	11
NG-15	38	423	0.09	0.068	0.002	1.318	0.023	0.142	0.002	853	66	854	12	854	10
NG-16	54	313	0.17	0.066	0.002	1.29	0.023	0.141	0.002	813	66	852	12	841	10
NG-17	72	206	0.35	0.068	0.002	1.332	0.025	0.142	0.002	873	66	854	12	860	11
NG-18	29	213	0.13	0.068	0.002	1.313	0.028	0.141	0.002	853	70	850	12	851	12

Table 2

Trace elements for the zircons from Nage porphyry.

Analysis spot	NG-1	NG-2	NG-3	NG-4	NG-5	NG-6	NG-7	NG-8	NG-9	NG-10	NG-11	NG-12	NG-13	NG-14	NG-15	NG-16	NG-17	NG-18
Ti	4.5	9.6	10.4	7.6	6.3	6.4	13.7	6.5	16.9	5.8	2.9	327	7.6	3.5	2.6	3.8	7.3	4.3
Y	2260	3078	2681	3379	1642	1752	3170	2069	2230	1470	1764	2841	1396	2178	2041	2172	1656	594
Nb	1.04	0.97	1.69	0.98	1.03	0.97	5.39	0.81	0.99	1.10	0.97	5.47	0.72	1.02	0.95	1.03	1.29	0.77
La	–	0.041	0.038	0.027	–	–	0.971	0.015	0.016	0.062	–	0.206	–	–	–	–	0.093	–
Ce	0.48	1.14	3.48	0.80	0.95	0.79	30.40	1.28	1.24	1.96	0.44	14.30	1.00	0.51	0.42	0.59	1.24	0.92
Pr	0.023	0.150	0.293	0.072	0.047	0.067	1.020	0.101	0.117	0.106	0.014	0.387	0.076	0.018	–	0.030	0.131	–
Nd	0.61	2.73	5.09	1.56	0.89	1.14	10.80	2.19	1.96	1.16	0.36	5.90	1.40	0.55	0.29	0.56	1.97	0.35
Sm	2.41	8.05	8.52	5.77	3.22	3.42	18.80	5.87	5.69	2.98	1.66	12.00	3.88	2.29	1.87	2.15	4.17	1.63
Eu	–	0.061	0.383	0.068	0.065	0.105	3.12	0.152	0.058	0.248	0.046	0.255	0.248	0.054	0.0531	0.069	0.202	0.061
Gd	21.3	53	52.4	42.2	22.6	23.7	85.5	37.2	34.3	21.8	15.6	63.8	28.5	20.5	17.5	22.1	26.6	13
Tb	11.9	22.3	20.4	20.7	10.1	10.9	30.6	14.9	15.1	10.0	8.8	23.1	11	11.3	10.2	11.4	11.3	5.5
Dy	174	281	248	286	139	148	322	189	193	130	133	274	130	169	158	169	145	58
Ho	77	110	97	118	58	62	104	75	79	51	61	105	52	77	70	76	61	20
Er	370	472	410	524	265	285	407	334	354	221	304	454	230	373	347	373	282	83
Tm	85	101	83	113	58	63	83	71	76	48	71	96	48	85	80	84	61	18
Yb	812	913	741	1018	557	601	725	671	712	467	706	898	469	825	794	819	596	166
Lu	146	159	130	179	101	110	125	123	128	88	133	162	91	155	150	156	116	31
Nb	1.04	0.97	1.69	0.98	1.03	0.97	5.39	0.81	0.99	1.10	0.97	5.47	0.72	1.02	0.95	1.03	1.29	0.77
Ta	0.705	0.484	0.695	0.561	0.564	0.548	2.165	0.46	0.561	0.693	0.835	1.849	0.242	0.83	0.898	0.814	0.546	0.443
Th	49	123	313	89	60	58	1222	97	107	64	37	663	58	51	38	54	72	29
U	342	249	368	372	202	206	891	241	296	319	322	626	125	355	423	313	206	213
<i>0 wt% H₂O</i>																		
log fO ₂	–26	–23	–21	–24	–23	–24	–18	–23	–21	–23	–27	–	–23	–26	–27	–26	–23	–24
ΔFMQ	–9	–8	–6	–8	–7	–8	–3	–7	–8	–6	–9	–	–7	–9	–9	–8	–7	–7
<i>1 wt% H₂O</i>																		
log fO ₂	–25	–22	–21	–23	–23	–23	–17	–23	–21	–22	–26	–	–22	–25	–26	–25	–22	–24
Δ FMQ	–8	–7	–6	–8	–7	–7	–3	–7	–7	–6	–8	–	–7	–8	–8	–7	–7	–7
<i>3 wt% H₂O</i>																		
log fO ₂	–24	–21	–20	–22	–22	–22	–16	–22	–20	–21	–25	–	–21	–24	–25	–24	–21	–23
ΔFMQ	–7	–6	–5	–7	–6	–6	–2	–6	–6	–5	–7	–	–6	–7	–7	–7	–6	–6
<i>6.5 wt% H₂O</i>																		
log fO ₂	–23	–20	–18	–21	–21	–21	–15	–20	–18	–20	–24	–	–20	–24	–23	–20	–21	–21
ΔFMQ	–6	–5	–3	–5	–5	–5	–1	–4	–5	–4	–6	–	–4	–6	–6	–5	–4	–4

Note: $\alpha\text{SiO}_2 = 1$, $\alpha\text{TiO}_2 = 0.63$, the Hf contents of zircon were calculated by using the Partition Coefficient from [Mahood and Hildreth, 1983](#).

5. Discussion

5.1. Effects of alteration on whole-rock compositions

Samples from the Nage granite porphyry have undergone some degree of alteration (Fig. 3). Petrographic examination identified some altered plagioclase in samples Nage-597, Nage-617, Nage-647, Nage-669, Nage-742, and Nage-747 (See Fig. 3f), whereas other samples contain relatively fresh plagioclase (Fig. 3e). Therefore, it is necessary to evaluate the effects of alteration on whole-rock compositions before we use them in the following discussion.

Many chemical weathering indices have been proposed, such as the CIA ([Nesbitt and Young, 1982](#)), CIW ([Harnois, 1988](#)) and PIA ([Fedo et al., 1995](#)), etc. All of them were developed based on the assumption that Al was relatively immobile during weathering ([Price and Velbel, 2000](#)). However, for the Nage granite porphyry, hydrothermal alteration may also play an important role. Recent research has shown that Al shows high mobility during hydrothermal alteration of deeply fractured granite ([Nishimoto and Yoshida, 2010](#)). Therefore, it is unsuitable to use these chemical weathering indices to evaluate the mobility of major and trace elements in the case of the Nage granite porphyry. For granite, TiO₂, Th, Nb, Ta, Zr and Hf have been proposed as immobile

Table 3
Lu-Hf isotope analyses for zircons from the Nage porphyry, southeastern Guizhou Province, South China (t = 850 Ma).

Sample	176Yb/177Hf	2σ	176Hf/177Hf	2σ	176Lu/177Hf	2σ	εHf(t)	T _{DM1}	2σ	T _{DM2}	2σ	f(Lu/Hf)
NG-01	0.077417	0.003413	0.282180	0.000023	0.001579	0.000038	–3.1	1536	64	1926	101	–0.95
NG-02	0.095319	0.001789	0.282187	0.000021	0.001863	0.000078	–3.0	1537	60	1919	94	–0.94
NG-03	0.099796	0.004042	0.282203	0.000019	0.002008	0.000042	–2.5	1521	55	1889	85	–0.94
NG-04	0.036974	0.006733	0.282158	0.000014	0.000759	0.000149	–3.4	1533	38	1945	60	–0.98
NG-05	0.092513	0.005419	0.282196	0.000020	0.001798	0.000062	–2.6	1523	57	1898	88	–0.95
NG-06	0.079614	0.003671	0.282196	0.000020	0.001652	0.000101	–2.6	1516	56	1892	88	–0.95
NG-07	0.066831	0.006184	0.282049	0.000037	0.001249	0.000083	–7.5	1706	103	2204	163	–0.96
NG-08	0.084046	0.003701	0.282175	0.000021	0.001729	0.000046	–3.3	1550	60	1942	94	–0.95
NG-09	0.098065	0.007364	0.282149	0.000026	0.001958	0.000100	–4.4	1596	73	2007	113	–0.94
NG-10	0.094263	0.005235	0.282163	0.000021	0.001854	0.000049	–3.8	1571	59	1972	92	–0.94
NG-11	0.092074	0.006630	0.282094	0.000037	0.001765	0.000075	–6.2	1666	106	2121	166	–0.95
NG-12	0.083911	0.004086	0.282222	0.000023	0.001688	0.000057	–1.6	1481	65	1836	101	–0.95
NG-13	0.099374	0.001844	0.282255	0.000029	0.001905	0.000059	–0.6	1442	84	1770	130	–0.94
NG-14	0.081729	0.003018	0.282162	0.000020	0.001607	0.000043	–3.7	1563	56	1966	87	–0.95
NG-15	0.142838	0.009002	0.282196	0.000031	0.002673	0.000203	–3.1	1558	89	1927	136	–0.92
NG-16	0.112959	0.004592	0.282199	0.000023	0.002132	0.000121	–2.7	1532	66	1903	102	–0.94

Table 4

Whole-rock Nd isotopic data for selected samples of Nage granite porphyry, southeastern Guizhou Province, South China.

Sample No.	Sm	Nd	$^{143}\text{Nd}/^{144}\text{Nd}$	2σ	$^{47}\text{Sm}/^{144}\text{Nd}$	$(^{143}\text{Nd}/^{144}\text{Nd})_i$	$\varepsilon\text{Nd (t)}$	$T_{\text{DM}} (\text{Ga})$	$T_{\text{2DM}} (\text{Ga})$
NG-597	7.38	36.6	0.511875	4	0.1219	0.511194	-6.7	2.1	1.9
NG-609	5.64	27.5	0.511899	4	0.1240	0.511206	-6.5	2.1	1.9
NG-647	8.01	41.4	0.511886	8	0.1169	0.511233	-6.0	2.0	1.8
NG-669	8.59	42.9	0.511897	4	0.1210	0.511221	-6.2	2.1	1.8
NG-685	6.35	32.3	0.511892	6	0.1188	0.511228	-6.1	2.0	1.8
NG-710	6.34	31.9	0.511883	4	0.1201	0.511212	-6.4	2.1	1.9
NG-733	7.26	36.7	0.511878	2	0.1196	0.511210	-6.4	2.1	1.9
NG-747	7.16	36.7	0.511876	4	0.1179	0.511217	-6.3	2.0	1.8

elements during chemical weathering and all subsequent alteration (Panahi et al., 2000). In this study, the TiO₂, Nb, Hf, Ta, Th and U show good correlations with Zr, which indicates that these elements were immobile (Fig. 7). As a consequence, we use selected major elements vs. TiO₂ and selected trace elements vs. Zr to evaluate the effect of alteration.

For the relatively fresh samples (with fresh plagioclase), the selected elements Fe₂O₃, MnO, MgO, K₂O, Nb, Y, Rb and Ba are well correlated with TiO₂ and Zr, whereas for those samples containing altered plagioclase, no such correlation was observed (except for the HFSE elements like Nb and Y; Fig. 8e, f). Therefore, only those immobile elements (HFSE elements like Nb, Th, Y, and REE) and relatively fresh samples were used in the following discussion.

5.2. I-, S- or A-type granites?

S-type granites have higher A/CNK (> 1.1) values than those of typical I-type granites (A/CNK < 1.1) because of leaching out of Na and Ca from sedimentary/supracrustal source rocks by alteration and weathering (Chappell and White, 1992). Generally, there are three major processes that can generate high A/CNK (Zen, 1988), i.e., 1) differentiation of metaluminous magma, whatever its origin, with or without assimilation; 2) late-stage, but super-solidus, metasomatic loss of alkalis through vapor phase transport; or 3) partial melting, especially of peraluminous sedimentary rocks. Fractional crystallization of hornblende can account for the development of peraluminous compositions (Cawthorn et al., 1976). However, as pointed out by subsequent studies, generation of peraluminous compositions by such a process is inefficient for large bodies of magma (Zen, 1988; Chappell, 1999). Furthermore, fractional crystallization of amphibole will cause depletion of MREE in the melt (e.g., Wu et al., 2014a), but this was not observed in the Nage granite porphyry (Fig. 6b). Alteration has played a limited role in the whole-rock geochemistry of the relatively fresh samples, because of the tight correlations between the major and trace

elements with TiO₂, Zr, respectively (Figs. 7 and 8). All samples have A/CNK greater than 1.1. Thus, high A/CNK values (> 1.1) in the samples from the Nage granite porphyry are most probably inherited from their source.

Typical A-type granites show high 10,000*Ca/Al ratios (> 2.5), FeO/(FeO + MgO) ratios (mostly > 0.8), and high Zr contents (> 250 ppm) (e.g., Whalen et al., 1987; Frost et al., 2001; Wu et al., 2014b). The Nage granite porphyry is not a A-type granite because of the low 10,000*Ca/Al (2.05–2.57), FeO/(FeO + MgO) ratios (0.6–0.8) and Zr contents (148–240 ppm). Their samples also plot out of the field of A-type granites in the (K₂O + Na₂O)/CaO and FeO/MgO vs. Zr + Nb + Ce + Y diagrams (Fig. 9a, b). They have low P₂O₅ (< 0.15 wt%) that decreases with increasing Rb content (Fig. 8i), which is a characteristic of I-type granites. Because previous studies have shown that the P₂O₅ contents of S-type granite would increase with increasing Rb, whereas those of I-type granites decreased (Chappell and White, 1992; Chappell et al., 1998). However, typical I-type granites, such as those from the Lachlan Fold Belt that were used to define I-type granites, have A/CNK lower than 1.1 (e.g., Chappell, 1999; Chappell and White, 2001). Therefore, the Nage porphyry granitoids cannot be typical I-type granites. Experimental petrology shows that peraluminous I-type melts can be generated by partial melting of metaluminous basaltic to andesitic rocks under crustal conditions (e.g., Beard and Lofgren, 1991; Patino Douce and Beard, 1995; Sisson et al., 2005). However, most of these melts have K₂O/Na₂O < 1 (Zhao et al., 2015 and references therein). Samples from the Nage granite porphyry exhibit high K₂O/Na₂O ratios (0.7–2.6; average 1.4), which is also inconsistent with such an interpretation. Additionally, some highly-fractionated I-type granites can also have A/CNK > 1.1 (Wu et al., 2003). However, nearly all of the samples plot outside of the field of fractionated granite (Fig. 9a, b). Therefore, their high A/CNK (> 1.1) and K₂O/Na₂O (0.7–2.6; average 1.4) ratios suggest a dominantly metasedimentary source.

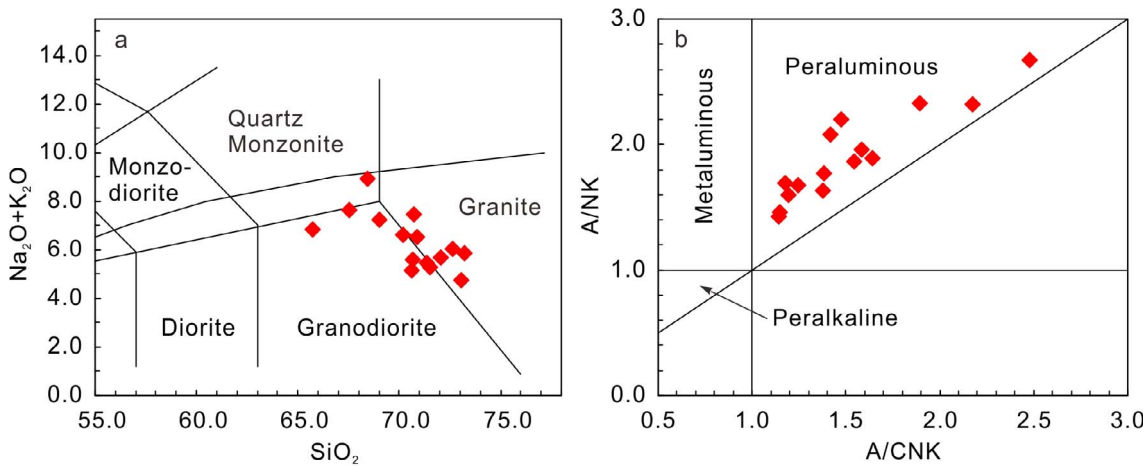


Fig. 5. (a) Total alkali vs. silica (TAS) diagram (after Le Bas et al., 1986) and (b) molar Al/(K + Na) vs. Al/(Ca + Na + K) diagram for the Nage granite porphyry.

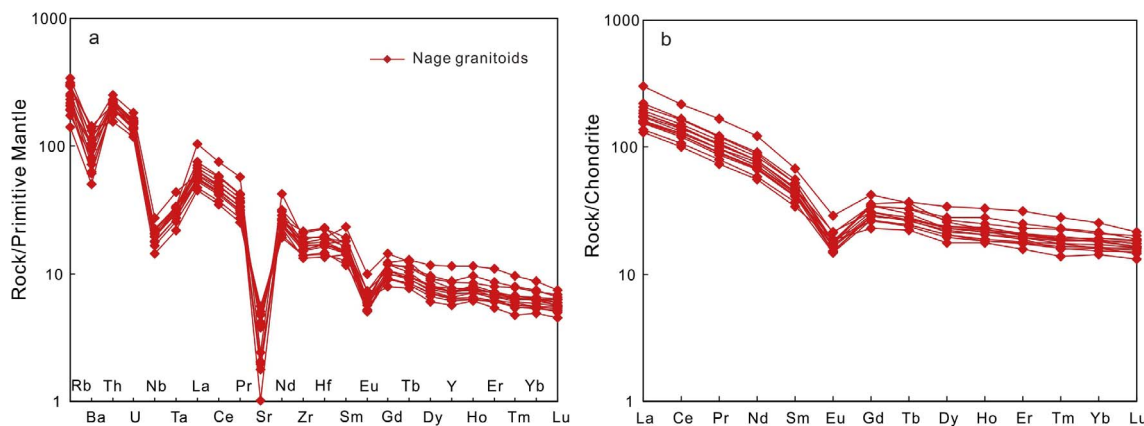


Fig. 6. (a) Primitive-mantle normalized trace element patterns and chondrite-normalized REE patterns of the Nage granite porphyry samples. Chondrite and primitive mantle-normalized values are from Sun and McDonough (1989).

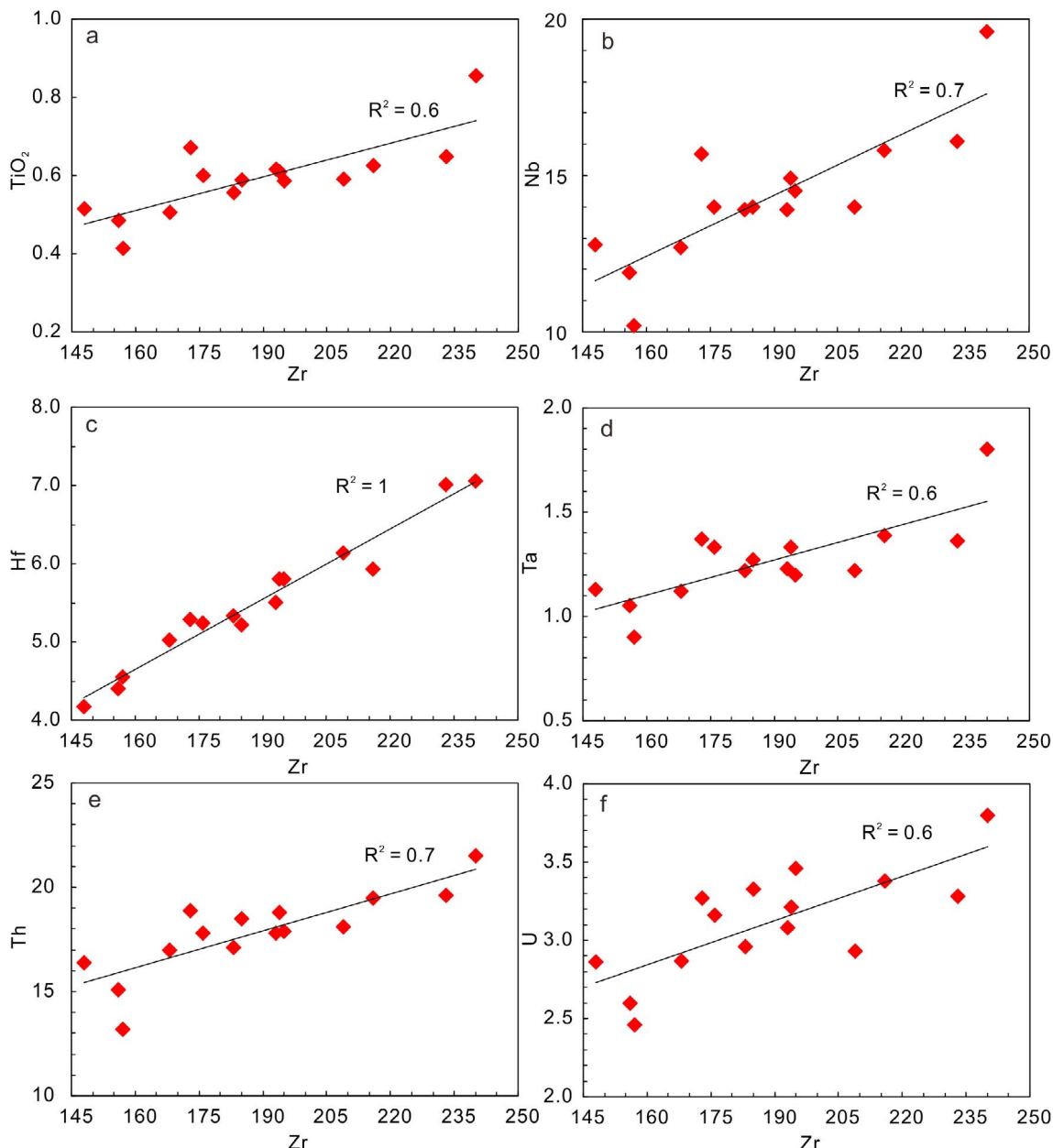


Fig. 7. Plots of TiO_2 , Nb , Hf , Ta , Th and U vs. Zr for the Nage granite porphyry. They are all well corrected with Zr .

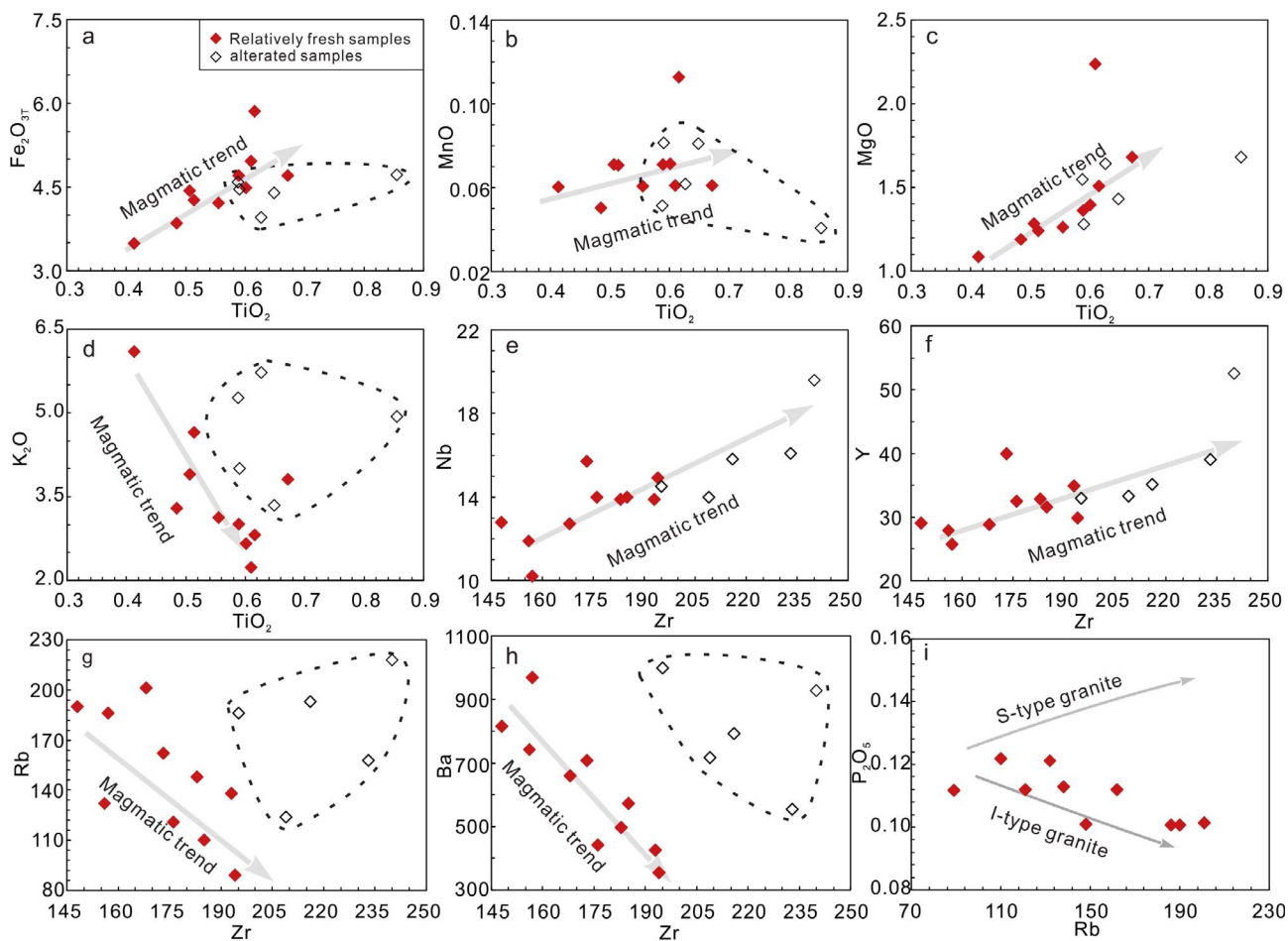


Fig. 8. (a)–(d) Plots of major, trace elements vs. TiO_2 and (e)–(h) plots of selected trace elements vs. Zr diagrams. (i) plot of P_2O_5 vs. Rb . The I- and S-type granite trends are from Chappell and White, 1992.

5.3. Magmatic conditions

Zircon saturation thermometry (T_{Zr}) provides a simple and robust way to estimate magma temperatures (Watson and Harrison, 1983). It was developed based on the observation that solubility of zircon is strongly sensitive to temperature and magma composition, but, in most cases, insensitive to other factors (Watson and Harrison, 1983; Hanchar and Watson, 2003; Miller et al., 2003). In our study, following the methods of Watson and Harrison (1983) and Miller et al. (2003), the Nage granite porphyry has relatively high zircon saturation

temperatures of $T_{\text{Zr}} = 786^{\circ}\text{C}$ to 842°C , mostly $> 810^{\circ}\text{C}$ (Table S1), similar to those of “hot granites” (Fig. 10; Miller et al., 2003). Combined with the observation that no inherited cores are present in the zircons from the Nage porphyry, it suggested that their primary magma may be Zr-undersaturated. In this case, the calculated T_{Zr} of the Nage porphyry provides a minimum estimate for magma temperature at a time before extensive crystallization, probably effectively upon emplacement (Miller et al., 2003). Oxygen fugacity ($f\text{O}_2$) is also an important thermodynamic parameter of magma (Arató and Audébat, 2017 and references therein). Recently, a newly developed Ce-in-zircon

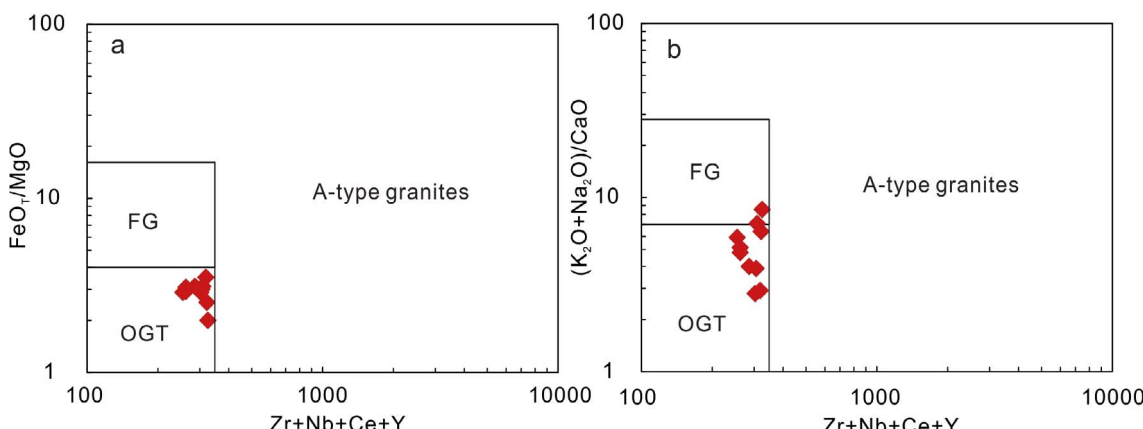


Fig. 9. A-type granite discriminant diagrams of (a) $\text{FeO}_{\text{T}}/\text{MgO}$ vs. $\text{Zr} + \text{Nb} + \text{Ce} + \text{Y}$, and (b) $(\text{K}_2\text{O} + \text{Na}_2\text{O})/\text{CaO}$ vs. $\text{Zr} + \text{Nb} + \text{Ce} + \text{Y}$ (after Whalen et al., 1987). FG: fractionated felsic granites; OGT: unfractionated M-, I- and S-type granites. Only the fresh samples are plotted.

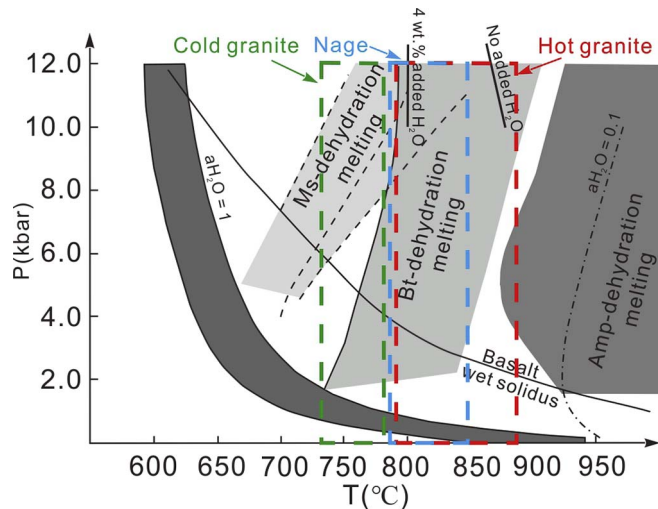


Fig. 10. P-T diagram showing the P-T conditions of muscovite, biotite and amphibole-dehydration melting (from Weinberg and Hasalová, 2015). The fields cold granites (766 ± 24 °C) and hot granites (837 ± 48 °C) are from Miller et al. (2003).

oxygen barometer (Smythe and Brenan, 2016) has been developed. If using this method, the water content of the granitic magma is needed. However, quantification of H_2O contents of natural granites has been an on-going challenge owing to the extremely fugitive character of H_2O during cooling and ascent of melts and magmas (Bartoli et al., 2014). Here, we use water-free (0 wt%), 1 wt%, 3 wt% and 6.5 wt% water contents to calculate the $f\text{O}_2$ of the porphyry samples. The results demonstrate that there are only small differences between them (Table 2). Therefore, the Nage granite porphyry has low $\log f\text{O}_2$ values ranging from -16 to -25 (3 wt% water), corresponding to $\Delta\text{FMQ} - 3$ to $\Delta\text{FMQ} - 7$, indicating a low oxygen fugacity (Table 2). Perple_X is widely used for constraining the crystallization conditions of metamorphic systems, however, it has also been successfully applied to granitic rocks (e.g., Clemens et al., 2011; Clemens and Phillips, 2014; Zhao et al., 2017). Here we also used the Perple_X thermodynamic modeling package (Connolly 2009; <http://www.perple.ethz.ch/>) to calculate the P-T mineral stability fields for the bulk composition of sample Nage-710. The models of minerals (feldspar, garnet, orthopyroxene, olivine, biotite, muscovite, cordierite and ilmenite) that were chosen in this study are the same as in Clemens et al., 2011. We calculated our sample under $\text{H}_2\text{O} = 1$ wt% and 3 wt% respectively (Fig. 11a, b). Although the Nage

granite porphyry shows strongly peraluminous affinities, common peraluminous minerals like garnet, cordierite and muscovite were not present in the rock. The mineral assemblage of Nage-710, as well as other samples from the Nage granitoids, is quartz + plagioclase + k-feldspar + biotite (Fig. 3). Therefore, if the thermodynamic modeling that we used is reliable, the mineral assemblage of Nage-710 suggests a low pressure (< 0.5 GPa) and narrow crystallization temperature conditions (640–680 °C; grey shaded area in Fig. 11a, b). It should be noted that T_{zr} provides minimum estimates of temperature Nage porphyry, whereas the crystallization temperature describes the temperature at which the minerals crystallized. They are two different parameters and will be discussed below. Based on the discussed above, the Nage granite porphyry has high T_{zr} but low $f\text{O}_2$, and was emplaced at middle-upper crust levels.

5.4. The effect of fractional crystallization on granitoid composition

Although the source is considered to be the primary control on granite magma chemistry (Clemens and Stevens, 2012), the geochemical composition of granitoids can also be determined by subsequent magmatic processes, such as magma mixing, fractional crystallization, and assimilation of country rocks, as well as the fundamental control of partial melting (Wu et al., 2017b; Zhao et al., 2015 and the references therein). Magma mixing is unlikely, because no mafic microgranular enclaves were observed in the drill core. As zircon is the major container of Zr, fractional crystallization of zircon would decrease the Zr concentration of the residual magma. Therefore, the T_{zr} calculated by whole-rock sample with different Zr concentrations can be used to trace the element variations during fractional crystallization. The errors that are generated in the original measurements (e.g., EMPA, XRF, etc.) used in the zircon saturation temperature calculation must be propagated through. However, as mentioned by Miller et al. (2003), the very strong temperature dependence of zircon solubility results in a highly robust geothermometer. Large errors in estimates of Zr and major element concentration (M) result in relatively small errors in calculated T_{zr} . For example, large uncertainties in melt composition (tonalite vs. leucogranite) only introduce small error in estimated temperature (Miller et al., 2003). As a consequence, the calculated T_{zr} of Nage granite porphyry (786–842 °C) can be used to trace the element variations during fractional crystallization.

As shown in Fig. 12a-c, the Fe_2O_3 , TiO_2 and MgO contents of the Nage granite porphyry decreased with decreasing T_{zr} , which suggested fractionation involving Fe-Ti oxides and some mafic minerals (e.g.,

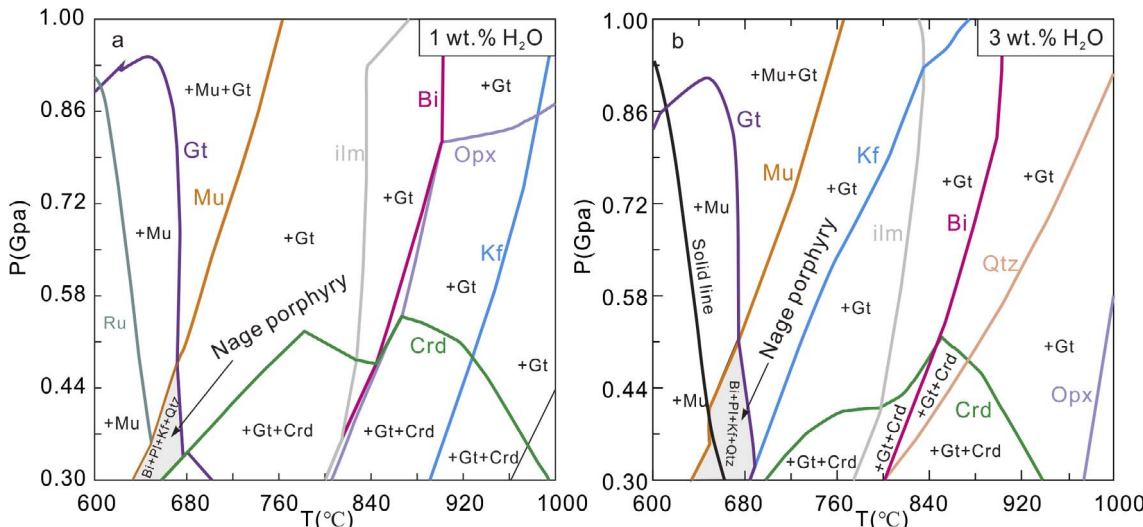


Fig. 11. P-T phase diagrams for sample Nage-710 from the Nage granite porphyry, calculated using Perple_X (Connolly, 2009) at (a) 1 wt% H_2O and (b) 3 wt% H_2O . Solid curves mark the phase stability fields. Phases are labeled inside their stability field. “+ A” means mineral A was stable in this field.

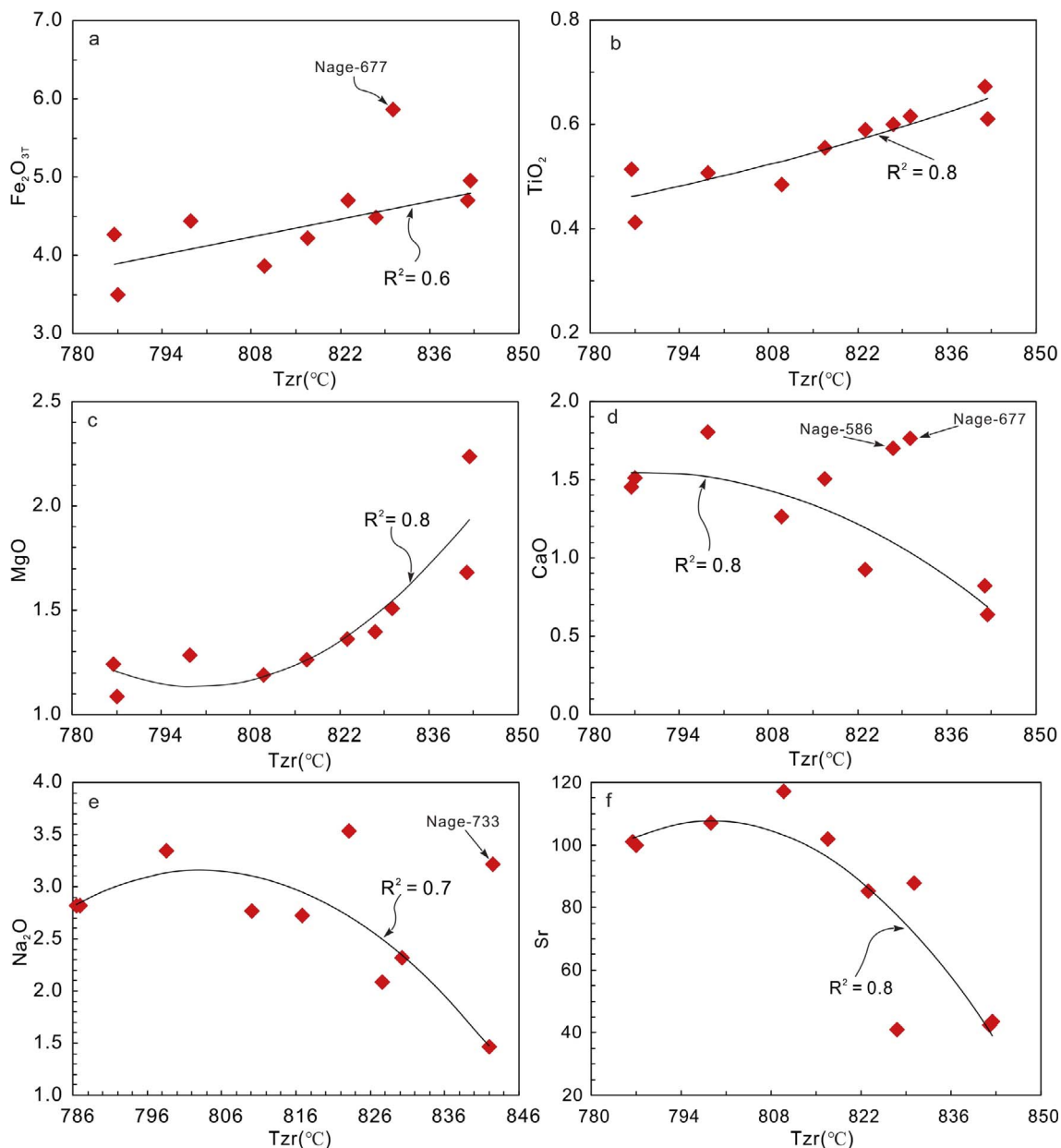


Fig. 12. Selected major and trace elements vs. T_{zr} . They are all well-correlated with T_{zr} . Only fresh samples are plotted. Correlations in (a), (d) and (e) were calculated without samples Nage-677, Nage-586, Nage-677, and Nage-733.

amphibole). However, CaO, Na₂O and Sr generally increased with decreasing T_{zr} (Fig. 12d, e and f), which indicates that the fractional fractionation of plagioclase was limited during the interval where magma temperatures were 780–850 °C. This is also confirmed by the Al₂O₃ contents, which slightly decreased and then increased with decreasing T_{zr} (Fig. 13a), because fractional fractionation of plagioclase will significantly decrease the Al₂O₃ content of the magma. Furthermore, the K₂O and Rb increased rapidly with decreasing magma temperature (Fig. 13b, c), which demonstrates that fractional crystallization of K-feldspar/biotite was also limited during this temperature interval. This can explain why the crystallization temperatures estimated from the mineral assemblage of quartz + plagioclase + K-feldspar + biotite (640–680 °C) are lower than the calculated T_{zr} (786–842 °C) and suggest that the thermodynamic modeling used above is valid.

Based on the study of Mesozoic granitic intrusions in the Nanling Range, southeastern Jiangxi Province, China, Zhao et al. (2015) found that the Triassic Caijiang pluton and Jurassic Huangpi, Daguzhai and

Luobuli plutons have similar source regions. However, because of the different T_{zr} , the high T_{zr} Triassic granitoids show A-type affinity, whereas the low T_{zr} Jurassic granitoids are similar to S-type granites. They proposed that melting temperature played an important role in dictating the composition of granitoids. In the case of the Nage granite porphyry, the Zr + Nb + Ce + Y values (maybe also the 1000*Ga/Al ratios) also show good correlations with T_{zr} (Fig. 13d and e). According to Whalen et al. (1987), A-type granites have Zr + Nb + Ce + Y values and 1000*Ga/Al ratios higher than 350 ppm and 2.5, respectively. As discussed above, the calculated T_{zr} of Nage granite porphyry samples provide a minimum estimate for the magma temperature. The primary magma may have had a magma temperature higher than 842 °C. Using the equation shown in Fig. 13d, the Zr + Nb + Ce + Y values rise to 350 ppm when $T_{zr} = 862$ °C. Therefore, the primary magma of the Nage granite porphyry may have had an A-type affinity. Previous studies have proposed that the behavior of Zr, REE, Y, Th, and U during felsic crustal processes is mostly controlled by four accessory minerals (monazite, xenotime, apatite and zircon) that usually account for at

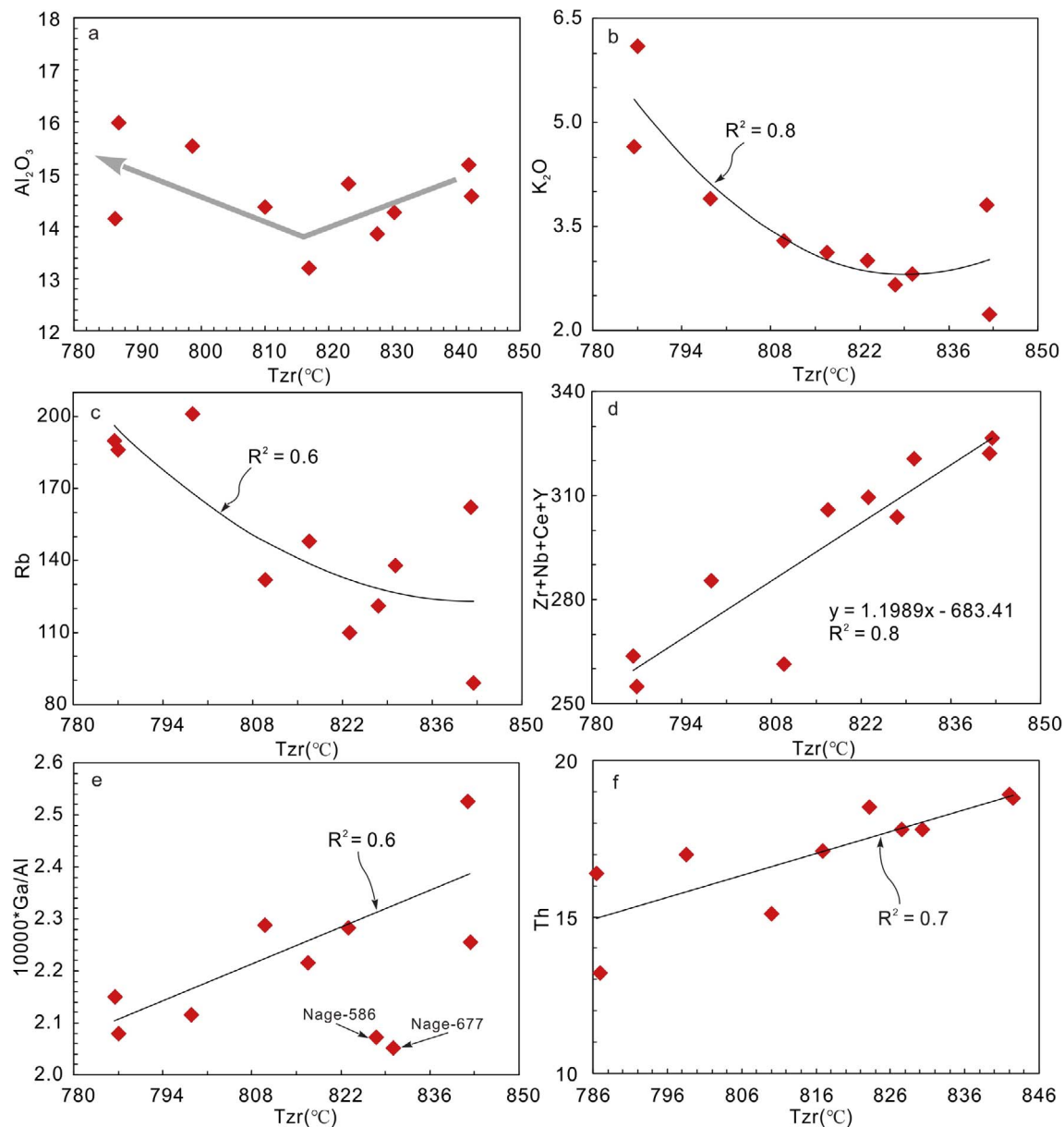


Fig. 13. Plots of oxides, elements and ratios against T_{zr} (°C). (a) Al_2O_3 vs. T_{zr} , (b) K_2O vs. T_{zr} , (c) Rb vs. T_{zr} , (d) $\text{Zr} + \text{Nb} + \text{Ce} + \text{Y}$ vs. T_{zr} , (e) $1000^*\text{Ga}/\text{Al}$ vs. T_{zr} and (f) Th vs. T_{zr} . Only fresh samples are plotted. The correlation in (e) was calculated without samples Nage-586 and Nage-677.

least 80–90% of the total budget of these elements in crustal rocks (e.g., Bea, 1996; Cámera et al., 2017). Therefore, the evolved magma may have lost these elements because of fractional crystallization of a certain amount of related accessory minerals at an early stage. Our study suggests that fractional crystallization may have played an important role in determining the composition of granitoid rocks such as the Nage granite porphyry.

5.5. Petrogenesis of the Nage granite porphyry

Previous studies have demonstrated that the petrogenesis of strongly peraluminous granitoids was extremely complicated. For example, partial melting of metasedimentary or metaigneous rocks, or a mixture of mantle-derived and crust-derived magma, all are possible mechanisms (e.g., Gray, 1984; Patiño Douce, 1995, 1999; Collins, 1996; Sylvester, 1998; Clemens, 2003; Healy et al., 2004; Peng et al., 2015; Zhao et al., 2015). As discussed above, the magma mixing model is unsuitable for the Nage granite porphyry and metasedimentary rocks

were likely dominant in the source. Furthermore, the Nage granite porphyry has Nd–Hf isotopes similar to the 825–815 Ma peraluminous granites in the study area (Fig. 14a, b). Previous studies proposed that these 825–815 Ma peraluminous granites in the central South China Block were derived from a mixed source that contains both ancient and young crustal materials (e.g., Wu et al., 2006; Zhao et al., 2013a,b; Wang et al., 2013). The $\epsilon_{\text{Nd}}(t)$ values of the Nage granite porphyry plot out of the area of metasediments from Kongling terrain (Fig. 14a), which are commonly considered as the basement of Yangtze Block (Gao et al., 1999). It's therefore reasonable to propose that, like the 825–815 granites in the study area, the source of Nage granite porphyry also contains some juvenile crustal materials. The $\text{CaO}/\text{Na}_2\text{O}$ ratios of strongly peraluminous granites can reflect the plagioclase/clay ratio of their source (Sylvester, 1998). Commonly, juvenile materials have high $\text{CaO}/\text{Na}_2\text{O}$ ratios. If the granitoid magma was derived from an ancient source, but mixed with magma derived from juvenile materials, the $\text{CaO}/\text{Na}_2\text{O}$ ratios calculated for the mixed magma may overestimate those of the source region. However, as discussed above, magma mixing

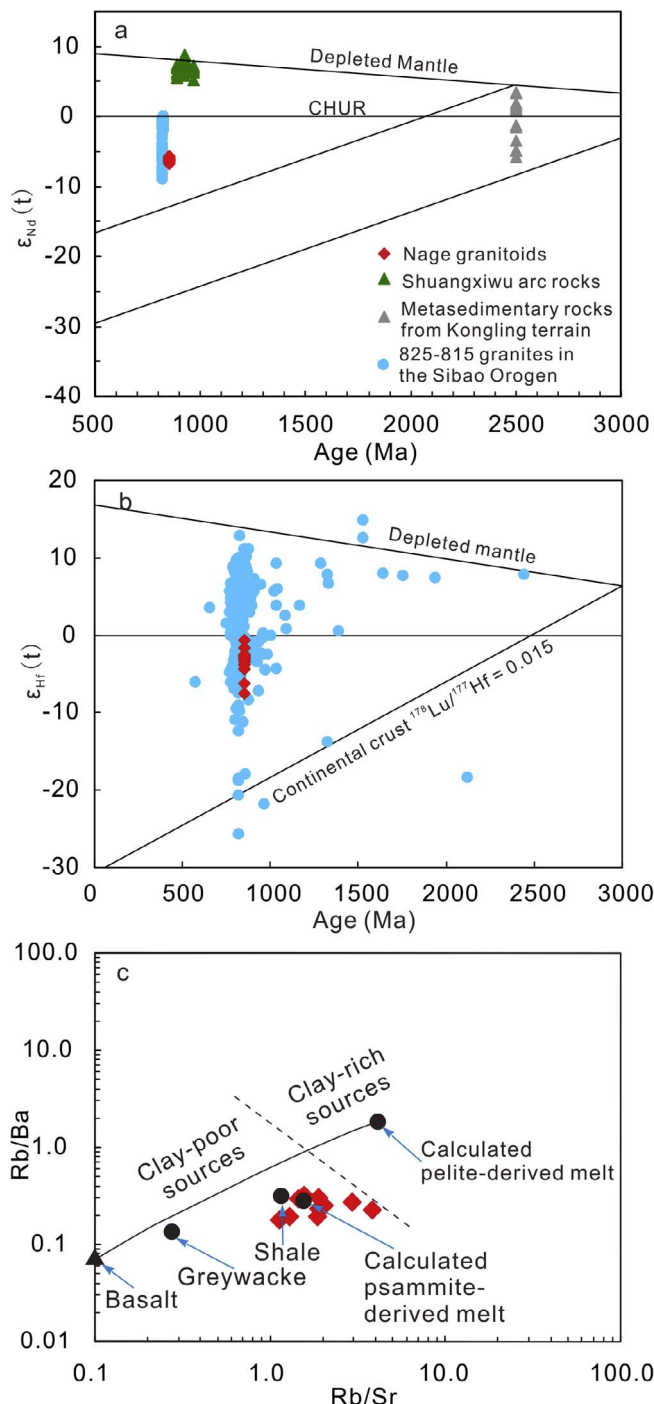


Fig. 14. Plots of (a) $\epsilon_{\text{Nd}}(t)$ vs. Age (Ma), (b) $\epsilon_{\text{Hf}}(t)$ vs. Age (Ma), (c) Rb/Ba vs. Rb/Sr (after Sylvester, 1998). Only fresh samples are plotted. Zircon Hf isotopic data for the 825–815 Ma granites in the Sibao Orogen are from Wu et al., 2006; Zhao et al., 2013a; Wang et al., 2013; Nd isotopic data for Shuangxiwu arc rocks are from Li, 1999; Metasedimentary rocks of the Kongling terrain are from Gao et al., 1999; 825–815 Ma granites in the Sibao Orogen are from Li et al., 2003; Wang et al., 2006; Wu et al., 2006.

is unlikely in the case of the Nage granite porphyry, and juvenile materials were likely a part of the source. Therefore, the CaO/Na₂O ratios may still reflect the plagioclase/clay ratios of the source region. Samples from the Nage granite porphyry have high CaO/Na₂O ratios ranging from 0.2 to 0.8 (mostly > 0.5; Table S1), suggesting a clay-poor source (Fig. 14c). The wide range of CaO/Na₂O ratios may reflect the source heterogeneous of the Nage granite porphyry.

Based on the discussion above, the fundamental observations for the

Nage granite porphyry are: 1) metasedimentary rocks were dominant in the source; 2) the source rocks were clay-poor and contained some juvenile materials; and 3) samples from the Nage granite porphyry show I-type affinity with low P₂O₅ contents that decreased with increasing Rb (Fig. 8i). Previous studies have proposed that granitic melts would show some I-type affinities when their source consisted of immature arkose and graywacke that had largely preserved their original igneous compositions (Zen, 1988; Miller, 1985; White et al., 1986). Such immature sedimentary rocks underwent some degree of weathering, which would likely result in the loss of a certain amount of Na and Ca relative to Al. As they may have largely preserved their original igneous compositions, partial melting would produce peraluminous magma but showing some I-type affinity (Zen, 1988 and references therein). Therefore, the source of the Nage granite porphyry may also have been dominated by immature arkose and greywacke that mainly consisted of igneous materials.

It is widely accepted that before the final collision between the Yangtze and Cathaysia blocks, the zone where the study area is located underwent a period of subduction, although the time of the subduction still remains controversial (e.g., Li et al., 2008a,b,c; Cawood et al., 2013; Zhao et al., 2015). It has been suggested that in a supra-subduction zone setting, the time interval between syn-collisional magmatism and deposition of its weathered clastics can be very short, generally less than several million years (Hawkins, 2003). Studies of granitoids in the Lachlan Fold Belt of southeastern Australia (Keay et al., 1999) and south Anhui Province, China (Wu et al., 2006) further provide evidence that young sediments consisting of weathered juvenile crust can become incorporated into the source of syntectonic granitoids in a very short time interval.

The Nage granite porphyry shows a close spatial relationship with the Sibao Group. The Sibao Group in the southwestern Yangtze Block is composed mainly of flysch turbidites (Wang et al., 2012b). Sandstones from the Sibao Group have intermediate to high SiO₂ (58.6–80.0 wt%) and extremely variable Al₂O₃ wt.% (7.4–20.6 wt%), typical of immature lithic varieties (Wang et al., 2012b). It is suggested that rocks of the Sibao Group have experienced intensive chemical weathering with extremely high A/CNK values (2–4.4; Wang et al., 2012b). Simple binary mixing between the basement rock and Neoproterozoic arc volcanic rocks shows that rocks of the Sibao Group may be composed of 60% juvenile crustal material and 40% ancient recycled crustal material (Fig. 15a). The samples from the Nage granite porphyry have similar geochemical features to those of the Sibao Group (Fig. 15b). Their uniform $\epsilon_{\text{Nd}}(t)$ values (−6.0 to −6.7) are also similar to those of the Sibao Group ($\epsilon_{\text{Nd}}(t = 852 \text{ Ma}) = -6.1$ to -7.3 ; Li and McCulloch, 1996). Thus, we propose that the Nage granite porphyry formed by anatexis of crustal rocks that had very similar geochemical compositions to those of the Sibao Group. However, this does not necessarily mean that these granitoids were directly derived from the Sibao Group. A similar situation also occurs for the ca. 825 Ma granitoids in south Anhui Province, in the southeastern Yangtze Block, which were considered to be derived from melting of arc-derived clastic sediments, similar to the neighboring Shangxi Group (Wu et al., 2006). Also, the late Paleozoic peraluminous granites of the eastern Urals were interpreted by Gerdes et al. (2002) as being related to relatively rapid rebuilding of juvenile arc crust together with deeply buried source rocks. In our study area, arc-continent or continent-continent collision may be the possible mechanism that caused the sediments derived from weathered juvenile arc crust to be mixed with ancient crustal materials that were strongly folded and deeply buried. Wu et al. (2006) used extensional collapse of the collisional orogen to explain the formation of the 825 Ma granitoids in south Anhui Province, by short-term recycling of juvenile crust (burial and melting). Such an extensional setting may have occurred at least as early as ca. 850 Ma in the study area.

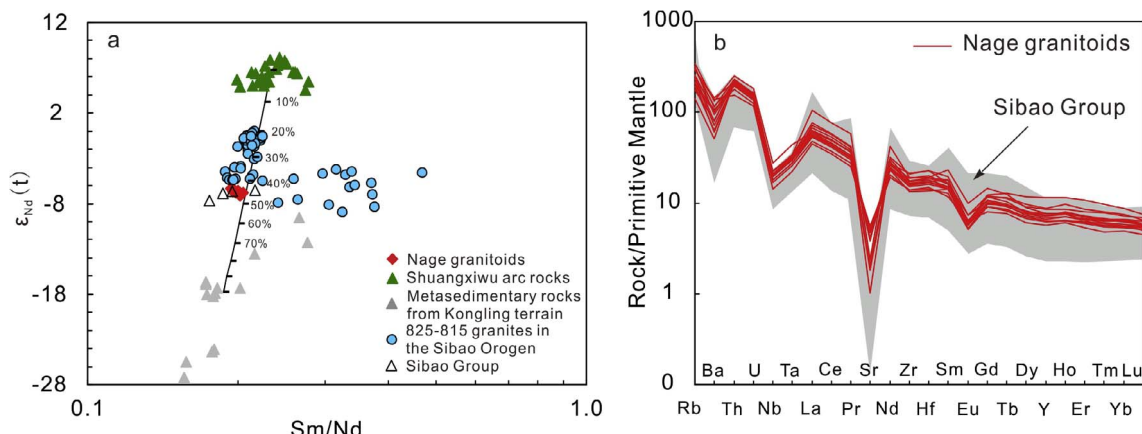


Fig. 15. (a) Simple binary mixing model shows the Sibao Group, as well as the source of Nage granite porphyry, consists of 60% juvenile crustal and 40% ancient recycled crustal material. The two end-members are the mean values of Shuangxiwu arc rocks and metasedimentary rocks of the Kongling terrane. The data sources are the same as in Fig. 14. (b) Comparing the geochemical data of the Nage granite porphyry samples with those of the Sibao Group in the primitive-mantle normalized trace element diagram. Data for the Sibao Group are from Li and McCulloch, 1996 and Wang et al., 2012a, 2012b.

5.6. Implications for ca. 850 Ma extension-related magmatism along the southern margin of the Yangtze Block

In the southeastern Yangtze Block, based on studies of the Shenwu dolerites (849 ± 7 Ma; Point 2 in Fig. 1b) and the Gangbian alkaline complex (848 ± 4 Ma; Point 3 in Fig. 1a), Li et al. (2010a,b) proposed that the ca. 850 Ma magmatism in this area occurred in an anorogenic setting related to either a post-orogenic event or the onset of Neoproterozoic continental rifting. Study on the Zhenzhushan Group (Point 6 in Fig. 1b) has also shown that the meta-volcanic rocks have bimodal signatures (849 ± 6 Ma; Li et al., 2010a,b). After summarizing coeval anorogenic magmatism in other blocks of the Rodinia supercontinent, Li et al. (2010a,b) further pointed out that these ca. 850 Ma anorogenic magmatic rocks may represent the early stage of the Rodinia superplume in response to a circum-Rodinia mantle avalanche after the complete assembly of the supercontinent. However, no anorogenic magmatism at this time has yet been reported in the central and southwestern Yangtze Block. Therefore, some researchers have proposed that the ca. 825–815 Ma strongly peraluminous granitoids formed in a post-extension setting that marked the final assembly of the SCB (e.g., Zhao et al., 2013a; Wang et al., 2014; Zhao, 2015 and references therein) and argued for an arc setting in these areas at ca. 850 Ma (e.g., Zhang et al., 2013; Yao et al., 2014; Zhao et al., 2015; Lin et al., 2016).

Strongly peraluminous granitoids are commonly generated in a post-collisional extensional setting (e.g., Sylvester, 1998; Peng et al., 2015), for example, in the European Alps (e.g., Altherr et al., 1995), the Caledonides (e.g., Searle et al., 1997), Hercynides (e.g., Finger et al., 1997), the Lachlan Fold Belt (e.g., Villaseca et al., 1998) and the Andean margins (e.g., Atherton, 1990). In this study, the high magma temperatures (786 – 842 °C, average 816 °C), low oxygen fugacity ($\Delta\text{FMQ} - 3$ to $\Delta\text{FMQ} - 7$), as well as the low emplacement pressure (< 0.5 GPa) of the Nage granite porphyry, also suggest an intraplate setting (e.g., Wu et al., 2016). Therefore, the “bimodal occurrence” of the ca. 850 Ma igneous rocks in the southwestern Yangtze Block and strongly peraluminous affinity of the Nage granite porphyry suggest that both the southeastern and southwestern margins of the Yangtze Block were under extension at ca. 850 Ma. The ca. 850 Ma anorogenic magmatism may be more widely distributed along the southern margin of Yangtze Block than previous proposed, but cannot be identified because of poor exposure. Therefore, the initial extension/rift along the southern margin of Yangtze Block may have formed as early as ca. 850 Ma. Such an scenario is also supported by other recent studies: 1) detrital zircon data from our study area indicate that sediments across the mid-Neoproterozoic unconformity shared similar sedimentary

provenances and were deposited within a similar tectonic setting, with both the Sibao and Danzhou groups most likely deposited in a continental rift basin (Yang et al., 2015); 2) a contemporaneous rift basin was initiated at ~ 860 Ma in the western Yangtze Block (Luojiamen conglomerates, our unpublished data); 3) ca. 870–700 Ma low $\delta^{18}\text{O}$ magmatism in the South China Block (Wang et al., 2011; Yang et al., 2015) indicates high-temperature water-rock interaction in a rift setting during this period; and 4) new geophysical data show that the Yangtze Block has a typical rift middle-lower continental crustal structure, which were interpreted as a rift basin developed at early Neoproterozoic (Dong et al., 2013, 2015).

Combined with the bimodal occurrence of other ca. 850 Ma intrusive rocks in the western part and the ca. 850 Ma Shuimo syenites in the northern parts of the Yangtze Block, ca. 850 Ma intraplate magmatism occurred widely throughout the entire Yangtze Block (Fig. 1b). These rocks are mostly distributed along the margins of the Yangtze Block, and most likely signify early continental rifting at ca. 850 Ma, probably corresponding to the initial break-up of the Rodinia supercontinent.

6. Conclusions

1. The newly identified 852 ± 5 Ma Nage granite porphyry has high A/CNK values (> 1.1) and zircon saturation temperatures, but low oxygen fugacity. Fractional crystallization may have played an important role in determining the geochemical composition.
2. The rocks have high $\text{K}_2\text{O}/\text{Na}_2\text{O}$ and $\text{CaO}/\text{Na}_2\text{O}$ ratios, and plot in the area of clay-poor sources in the Rb/Ba vs. Rb/Sr plot. They also have low P_2O_5 contents that decrease with increasing Rb . Combined with the zircon Hf and whole-rock Nd isotopes, we propose that the porphyry was derived from partial melting of a mixed source that consisted of weathered juvenile crust and ancient recycled crustal materials.
3. The porphyry was generated in an extensional setting. When combined with the ca. 850 Ma extension-related magmatism in the southeastern margin of Yangtze Block, the initial extension/rifting along the southern margin of Yangtze Block may have occurred as early as ca. 850 Ma.

Acknowledgements

This study was jointly supported by the Cooperation Project between the 102 Geological Team and the State Key Laboratory of Ore Deposit Geochemistry (SKLOGD, 2009–2013), the Science and Technology Foundation of Guizhou Province (2012–2334), the

National Basic Research Program of China (2014CB440905), the National Natural Science Foundation of China (41702047), an ARC Future Fellowship (FT140100826) to X.C. Wang, and a Visiting Scholar Project of the China Scholarship Council to J.-X. Zhou (201604910455). We are grateful for the constructive comments by two anonymous reviewers. We thank Profs. Mei-Fu Zhou, Yan Tao and Zhi-Long Huang for useful discussions and constructive suggestions.

Appendix A. Supplementary data

Supplementary data associated with this article can be found, in the online version, at <http://dx.doi.org/10.1016/j.precamres.2018.02.007>.

References

- Altherr, R., Lugovic, B., Meyer, H.-P., Majer, V., 1995. Early Miocene post-collisional calc-alkaline magmatism along the easternmost segment of the Periadriatic fault system (Slovenia and Croatia). *Mineral. Petrol.* 54, 225–247.
- Arató, R., Audétat, A., 2017. Vanadium magnetite-melt oxybarometry of natural, silicic magmas: a comparison of various oxybarometers and thermometers. *Contrib. Mineral. Petrol.* 172, 52.
- Atherton, M.P., 1990. The Coastal Batholith of Peru: the product of rapid recycling of 'new' crust formed within rifted continental margin. *Geol. J.* 25, 337–350.
- Bao, Z.W., Wang, Q., Bai, G.D., Zhao, Z.H., Song, Y.W., Liu, X.M., 2008. Geochronology and geochemistry of the Fangcheng Neoproterozoic alkali-syenites in East Qinling orogen and its geodynamic implications. *Chin. Sci. Bull.* 53, 2050–2061.
- Bartoli, O., Cesare, B., Remusat, L., Acosta-Vigil, A., Poli, S., 2014. The H_2O content of granite embryos. *Earth Planet. Sci. Lett.* 395, 281–290.
- Bea, F., 1996. Residence of REE, Y, Th and U in granites and crustal protoliths: implications for the chemistry of crustal melts. *J. Petrol.* 37, 521–552.
- Beard, J., Lofgren, G., 1991. Dehydration melting and water-saturated melting of basaltic and adesitic greenstones and amphibolites at 1, 3 and 6.9 kb. *J. Petrol.* 32, 365–402.
- Cámera, M.M.M., Dahlquist, J.A., Basei, M.A.S., Galindo, C., Neto, M.D.C.C.N., Facetti, N., 2017. Frich strongly peraluminous A-type magmatism in the pre-Andean foreland Sierras Pampeanas, Argentina: geochemical, geochronological, isotopic constraints and petrogenesis. *Lithos* 277, 210–227.
- Cawood, P.A., Wang, Y.J., Xu, Y.J., Zhao, G.C., 2013. Locating South China in Rodinia and Gondwana: a fragment of greater India lithosphere? *Geology* 41, 903–906.
- Cawthorn, R.G., Strong, D.F., Brown, P.A., 1976. Origin of corundum-normative intrusive and extrusive magmas. *Nature* 259, 102–104.
- Chappell, B.W., 1999. Aluminium saturation in I- and S-type granites and the characterization of fractionated haplogranites. *Lithos* 46, 535–551.
- Chappell, B.W., White, A.J.R., 1992. I- and S-type granites in the Lachlan Fold Belt. *Trans. R. Soc. Edinburg: Earth Sci.* 83, 1–26.
- Chappell, B.W., White, A.J.R., 2001. Two contrasting granite types: 25 years later. *Aust. J. Earth Sci.* 48, 489–499.
- Chappell, B.W., Bryant, C.J., Wyborn, D., White, A.J.R., Williams, I.S., 1998. High- and low-temperature I-type granites. *Resour. Geol.* 48 (4), 225–235.
- Chappell, B.W., Bryant, C.J., Wyborn, D., 2012. Peraluminous I-type granites. *Lithos* 153, 142–153.
- Clemens, J.D., 2003. S-type granitic magmas-petrogenetic issues, models and evidence. *Earth Sci. Rev.* 61, 1–18.
- Clemens, J.D., Phillips, G.N., 2014. Inferring a deep-crustal source terrane from a high-level granitic pluton: the Strathbogie Batholith, Australia. *Contrib. Mineral. Petrol.* 168, 1070.
- Clemens, J.D., Stevens, G., 2012. What controls chemical variation in granitic magmas? *Lithos* 134–135, 317–329.
- Clemens, J.D., Birch, W.D., Dudley, R.A., 2011. S-type ignimbrites with polybaric crystallisation histories: the Tolmie Igneous Complex, Central Victoria, Australia. *Contrib. Mineral. Petrol.* 162, 1315–1337.
- Collins, W.J., 1996. Lachlan Fold Belt granitoids: products of three-component mixing. *Trans. R. Soc. Edinburg: Earth Sci.* 87, 171–181.
- Connolly, J.A.D., 2009. The geodynamic equation of state: what and how. *Geochem. Geophys. Geosyst.* 10 (10).
- Dong, S.W., Gao, R., Yin, A., Guo, T.L., Zhang, Y.Q., Hu, J.M., Li, J.H., Shi, W., Li, Q.S., 2013. What drove continued continent-continent convergence after ocean closure? Insights from high-resolution seismic reflection profiling across the Daba Shan in central China. *Geology* 41 (6), 671–674.
- Dong, S.W., Zhang, Y.Q., Gao, R., Su, J.B., Liu, M., Li, J.H., 2015. A possible buried Paleoproterozoic collisional orogen beneath central South China: evidence from seismic-reflection profiling. *Precambr. Res.* 264, 1–10.
- Du, L.L., Guo, J.H., Nutman, A.P., Wyman, D., Geng, Y.S., Yang, C.H., Liu, F.L., Ren, L.D., Zhou, X.W., 2014. Implications for Rodinia reconstructions for the initiation of Neoproterozoic subduction at ~860 Ma on the western margin of the Yangtze Block: evidence from the Guandaoshan Pluton. *Lithos* 196–197, 67–82.
- Fedo, C.M., Nesbitt, H.W., Young, G.M., 1995. Unraveling the effects of potassium metasomatism in sedimentary rocks and paleosols, with implications for paleo-weathering conditions and provenance. *Geology* 23, 921–924.
- Finger, F., Roberts, M.P., Haunschmid, B., Schermaier, A., Steyrer, H.P., 1997. Variscan granitoids of central Europe: their typology, potential sources and tectonothermal relations. *Mineral. Petrol.* 61, 67–96.
- Frost, B.R., Barnes, C.G., Collins, W.J., Arculus, R.J., Ellis, D.J., Frost, C.D., 2001. A geochemical classification for granitic rocks. *J. Petrol.* 42 (11), 2033–2048.
- Gan, B.P., Lai, S.C., Qin, J.F., Zhu, R.Z., Zhao, S.W., Li, T., 2016. Neoproterozoic alkaline intrusive complex in the northwestern Yangtze Block, Micang Mountains region, South China: petrogenesis and tectonic significance. *Int. Geol. Rev.* 59 (3), 311–332.
- Gao, S., Ling, W.L., Qiu, Y.M., Zhou, L., Hartmann, G., Simon, K., 1999. Contrasting geochemical and Sm-Nd isotopic compositions of Archean metasediments from the Kongling high-grade terrain of the Yangtze craton: evidence for cratonic evolution and redistribution of REE during crustal anatexis. *Geochim. Cosmochim. Acta* 63 (13/14), 2071–2088.
- Gerdes, A., Montero, P., Bea, F., Ferschater, G., Borodina, N., Osipova, T., Shardakova, G., 2002. Peraluminous granites frequently with mantle-like isotope compositions: the continental-type Murzinke and Dzhabyk batholiths of the eastern Urals. *Int. J. Earth Sci.* 91, 3–19.
- Gray, C.M., 1984. An isotopic mixing model for the origin of granitic rocks in south-eastern Australia. *Earth Planet. Sci. Lett.* 70, 47–60.
- Guo, J.L., Gao, S., Wu, Y.B., Li, M., Chen, K., Hu, Z.C., Liang, Z.W., Liu, Y.S., Zhou, L., Zong, K.Q., Zhang, W., Chen, H.H., 2014. 3.45 Ga granitic gneisses from the Yangtze Craton, South China: implications for early Archean crustal growth. *Precambr. Res.* 242, 82–95.
- Hanchar, J.M., Watson, E.B., 2003. Zircon saturation thermometry. *Rev. Mineral. Geochim.* 53, 89–112.
- Harnois, L., 1988. The CIW index: a new chemical index of weathering. *Sediment. Geol.* 55, 319–322.
- Hawkins, J.W., 2003. Geology of supra-subduction zones - Implications for the origin of ophiolites. In: Dilek, Y., Newcomb, S. (Eds.), *Ophiolite Concept and the Evolution of Geological Thought*: Boulder. *Geol. Soc. Am. Spec.*, Colorado, pp. 227–268 Paper 373.
- Healy, B., Collins, W.J., Richards, S.W., 2004. A hybrid origin for Lachlan S-type granites: the Murrambeege Batholith example. *Lithos* 78, 197–216.
- Hu, Z.C., Liu, Y.S., Chen, L., Zhou, L., Li, M., Zong, K.Q., Zhu, L.Y., Gao, S., 2011. Contrasting matrix induced elemental fractionation in NIST SRM and rock glasses during laser ablation ICP-MS analysis at high spatial resolution. *J. Anal. At. Spectrom.* 26 (2), 425–430.
- Hu, Z.C., Liu, Y.S., Gao, S., Liu, W.G., Zhang, W., Tong, X.R., Lin, L., Zong, K.Q., Li, M., Chen, H.H., Zhou, L., Yang, L., 2012. Improved in situ Hf isotope ratio analysis of zircon using newly designed X skimmer cone and jet sample cone in combination with the addition of nitrogen by laser ablation multiple collector ICP-MS. *J. Anal. At. Spectrom.* 27, 1391–1399.
- Keay, S., Steele, D., Compston, W., 1999. Identifying granite sources by SHRIMP U-Pb zircon geochronology: an application to the Lachlan fold belt. *Contrib. Miner. Petrol.* 137, 323–341.
- Lai, S.C., Qing, J.F., Zhu, R.Z., Zhao, S.W., 2015. Petrogenesis and tectonic implication of the Neoproterozoic peraluminous granitoids from the Tianquan area, western Yangtze Block, South China. *Acta Petrol. Sin.* 31 (8), 2245–2258 (in Chinese with English abstract).
- Le Bas, M.J., Le Maître, R.W., Streckeisen, A., Zanettin, B., 1986. A chemical classification of volcanic rocks based on the total alkali-silica diagram. *J. Petrol.* 27, 745–750.
- Li, X.H., 1999. U-Pb zircon ages of granites from the southern margin of the Yangtze Block: timing of Neoproterozoic Jinning: orogeny in SE China and implications for Rodinia assembly. *Precambr. Res.* 97, 43–57.
- Li, X.H., McCulloch, M.T., 1996. Secular variations in the Nd isotopic composition of Late Proterozoic sediments from the southern margin of the Yangtze Block: evidence for a Proterozoic continental collision in SE China. *Precambr. Res.* 76, 67–76.
- Li, X.H., Zhang, L.H., Powell, C.M.C.A., 1995. South China in Rodinia: part of the missing link between Australia-East Antarctica and Laurentia? *Geology* 23, 407–410.
- Li, Z.X., Li, X.H., Zhou, H.W., Kinny, P.D., 2002. Grenvillian continental collision in south China: new SHRIMP U-Pb zircon results and implications for the configuration of Rodinia. *Geology* 30, 163–166.
- Li, X.H., Li, Z.X., Ge, W.C., Zhou, H.W., Li, W.X., Liu, Y., Wingate, M.T.D., 2003. Neoproterozoic granitoids in South China: crustal melting above a mantle plume at ca. 825 Ma? *Precambr. Res.* 122, 45–83.
- Li, Z.X., Li, X.H., Kinny, P.D., Wang, J., Zhang, S., Zhou, H., 2003. Geochronology of Neoproterozoic syn-rift magmatism in the Yangtze Craton, South China and correlations with other continents: evidence for a mantle superplume that broke up Rodinia. *Precambr. Res.* 122, 85–109.
- Li, X.H., Li, Z.X., Sinclair, J.A., Li, W.X., Carter, G., 2006. Revisiting the "Yanbian Terrane": implications for Neoproterozoic tectonic evolution of the western Yangtze Block, South China. *Precambr. Res.* 151, 14–30.
- Li, Z.X., Wartho, J.A., Occhipinti, S., Zhang, C.L., Li, X.H., Wang, J., Bao, C.M., 2007. Early history of the eastern Sibao Orogen (South China) during the assembly of Rodinia: new mica $^{40}\text{Ar}/^{39}\text{Ar}$ dating and SHRIMP U-Pb detrital zircon provenance constraints. *Precambr. Res.* 159, 79–94.
- Li, W.X., Li, X.H., Li, Z.X., 2008a. Middle Neoproterozoic syn-rifting volcanic rocks in Guangfeng, South China: petrogenesis and tectonic significance. *Geol. Mag.* 145, 475–489.
- Li, X.H., Li, W.X., Li, Z.X., Liu, Y., 2008b. 850–790 Ma bimodal volcanic and intrusive rocks in northern Zhejiang, South China: a major episode of continental rift magmatism during the breakup of Rodinia. *Lithos* 102, 341–357.
- Li, Z.X., Bogdanova, S.V., Collins, A.S., Davidson, A., De Waele, B., Ernst, R.E., Fitzsimons, I.C.W., Fuck, R.A., Gladkochub, D.P., Jacobs, J., Karlstrom, K.E., Lu, S., Natapov, L.M., Pease, V., Pisarevsky, S.A., Thrane, K., Vernikovsky, V., 2008c. Assembly, configuration, and break-up history of Rodinia: a synthesis. *Precambr. Res.* 160, 179–210.
- Li, X.H., Li, W.X., Li, Z.X., Lo, C.H., Wang, J., Ye, M.F., Yang, Y.H., 2009. Amalgamation

- between the Yangtze and Cathaysia Blocks in South China: constraints from SHRIMP U-Pb zircon ages, geochemistry and Nd-Hf isotopes of the Shuangxiwu volcanic rocks. *Precambr. Res.* 174, 117–128.
- Li, W.X., Li, X.H., Li, Z.X., 2010a. Ca. 850 Ma bimodal volcanic rocks in northeastern Jiangxi Province, South China: initial extension during the breakup of Rodinia? *Am. J. Sci.* 310, 951–980.
- Li, X.H., Li, W.X., Li, Z.X., Lo, C.H., Wang, J., Ye, M.F., Yang, Y.H., 2010b. Petrogenesis and tectonic significance of the ~850 Ma Gangbian alkaline complex in South China: evidence from *in situ* zircon U-Pb dating, Hf-O isotopes and whole-rock geochemistry. *Lithos* 114, 1–15.
- Lin, M.S., Peng, S.B., Jiang, X.F., Polat, A., Kusky, T., Wang, Q., Deng, H., 2016. Geochemistry, petrogenesis and tectonic setting of Neoproterozoic mafic-ultramafic rocks from the western Jiangnan orogen, South China. *Precambr. Res.* 35 388–356.
- Liu, X.M., Gao, S., Diwu, C.R., Ling, W.L., 2008. Precambrian crustal growth of Yangtze Craton as revealed by detrital zircon studies. *Am. J. Sci.* 308, 421–468.
- Liu, Y.S., Hu, Z.C., Zong, K.Q., Gao, C.G., Gao, S., Xu, J., Chen, H.H., 2010. Reappraisal and refinement of zircon U-Pb isotope and trace element analyses by LA-ICP-MS. *Chin. Sci. Bull.* 55, 1535–1546.
- Liu, Z., Jiang, Y.H., Wang, G.C., Ni, C.Y., Qing, L., Zhang, Q., 2015. Middle Neoproterozoic (~845 Ma) continental arc magmatism along the northwest side of the Jiangshan-Shaoxing suture, South China: geochronology, geochemistry, petrogenesis and tectonic implications. *Precambr. Res.* 268, 212–226.
- Ludwig, K.R., 2003. Isoplot 3.00, A Geochronological Toolkit for Microsoft Excel. Berkeley Geochronol. Center Spec. Publ., 1–70.
- Lyu, P.L., Li, W.X., Wang, X.C., Pang, C.J., Cheng, J.X., Li, X.H., 2017. Initial breakup of supercontinent Rodinia as recorded by ca 860–840 Ma bimodal volcanism along the southeastern margin of the Yangtze Block, South China. *Precambr. Res.* 296, 148–167.
- Mahood, G., Hildreth, W., 1983. Large partition coefficients for trace elements in high-silica rhyolites. *Geochim. Cosmochim. Acta* 47, 11–30.
- Meng, E., Liu, F.L., Du, L.L., Liu, P.H., Liu, J.H., 2015. Petrogenesis and tectonic significance of the Baoxing granitic and mafic intrusions, southwestern China: evidence from zircon U-Pb dating and Lu-Hf isotopes, and whole-rock geochemistry. *Gondwana Res.* 28, 800–815.
- Miller, C.F., 1985. Are strongly peraluminous magmas derived from pelitic sedimentary sources? *J. Geol.* 93, 673–689.
- Miller, C.F., McDowell, S.M., Mapes, R.W., 2003. Hot and cold granites? Implications of zircon saturation temperatures and preservation of inheritance. *Geology* 31, 529–532.
- Nesbitt, H.W., Young, G.M., 1982. Early Proterozoic climates and plate motions inferred from major element chemistry of lutites. *Nature* 299, 715–717.
- Nishimoto, S., Yoshida, H., 2010. Hydrothermal alteration of deep fractured granite: effects of dissolution and precipitation. *Lithos* 115, 153–162.
- Panahi, A., Young, G.M., Rainbird, R.H., 2000. Behavior of major and trace elements (including REE) during Paleoproterozoic pedogenesis and diagenetic alteration of an Archean granite near Ville Marie, Quebec, Canada. *Geochim. Cosmochim. Acta* 64, 2199–2220.
- Patino Douce, A.E., 1995. Experimental generation of hybrid silicic melts by reaction of high-Al basalt with metamorphic rocks. *J. Geophys. Res.* 100, 15623–15639.
- Patino Douce, A.E., 1999. What do experiments tell us about the relative contributions of crust and mantle to the origin of granitic magmas? In: Castro, A., Fernandez, C., Vigneresse, J.L. (Eds.), *Understanding Granites: Integrating New and Classical Techniques*. Spec. Publ. 168. Geol. Soc. London, pp. 55–75.
- Patino Douce, A.E., Beard, J.S., 1995. Dehydration-melting of bionite gneiss and quartz amphibolite from 3 to 15 kbar. *J. Petrol.* 36, 707–738.
- Peng, T.P., Fan, W.M., Zhao, G.C., Peng, B.X., Xia, X.P., Mao, Y.S., 2015. Petrogenesis of the early Paleozoic strongly peraluminous granites in the Western South China Block and its tectonic implications. *J. Asian Earth Sci.* 98, 399–420.
- Price, J.R., Velbel, M.A., 2000. Weathering of the Eaton Sandstone (Pennsylvanian), Grand Ledge, Michigan: geochemical mass balance and implications for reservoir properties beneath unconformities. *J. Sediment. Res.* 70, 1118–1128.
- Qi, L., Hu, J., Grégoire, D.C., 2000. Determination of trace elements in granites by inductively coupled plasma mass spectrometry. *Talanta* 51, 507–513.
- Qiu, Y.M., Gao, S., McNaughton, N.J., Groves, D.I., Ling, W.L., 2000. First evidence of > 3.2 Ga continental crust in the Yangtze craton of south China and its implications for Archean crustal evolution and Phanerozoic tectonics. *Geology* 28, 11–14.
- Searle, M.P., Parrish, R.R., Hodges, K.V., Hurford, A., Ayres, M.W., Whitehouse, M.J., 1997. Shisha Pangma leucogranite, south Tibetan Himalaya: field relations, geochemistry, age, origin, and emplacement. *J. Geol.* 105, 295–317.
- Shen, W.Z., Gao, J.F., Xu, S.J., Zhou, G.Q., 2002. Geochemical characteristics and genesis of the Qiaotou basic complex, Luding County, Western Yangtze Block. *Geol. J. China Univ.* 8 (4), 380–389 (in Chinese with English abstract).
- Sisson, T.W., Ratajeski, K., Hankins, W.B., Glazner, A.F., 2005. Voluminous granitic magmas from common basaltic sources. *Contrib. Mineral. Petro.* 148, 635–661.
- Smythe, D.J., Brenan, J.M., 2016. Magmatic oxygen fugacity estimated using zircon-melt partitioning of cerium. *Earth Planet. Sci. Lett.* 453, 260–266.
- Sun, S.S., McDonough, W.F., 1989. Chemical and isotopic systematics of oceanic basalts: implications for mantle composition and processes. In: Saunders, A.D., Norry, M.J. (Eds.), *Magmatism in the Ocean Basins*. Spec. Publ. 41. Geol. Soc. London, pp. 313–345.
- Sylvester, P.J., 1998. Post-collisional strongly peraluminous granites. *Lithos* 45, 29–44.
- Villaseca, C., Barbero, L., Herreros, V., 1998. A re-examination of the typology of peraluminous granite types in intracontinental orogenic belts. *Trans. R. Soc. Edinburg: Earth Sci.* 89, 113–119.
- Wang, X.L., Zhou, J.C., Qiu, J.S., Zhang, W.L., Liu, X.M., Zhang, G.L., 2006. LA-ICP-MS U-Pb zircon geochronology of the Neoproterozoic igneous rocks from Northern Guangxi, South China: implications for tectonic evolution. *Precambr. Res.* 145, 111–130.
- Wang, X.C., Li, X.H., Li, W.X., Li, Z.X., 2007. Ca. 825 Ma komatiitic basalts in South China: first evidence for > 1500 °C mantle melts by a Rodonian mantle plume. *Geology* 35 (12), 1103–1106.
- Wang, X.C., Li, X.H., Li, W.X., Li, Z.X., Liu, Y., Yang, Y.H., Liang, X.R., Tu, X.L., 2008. The Bikou basalts in the northwestern Yangtze block, South China: remnants of 820–810 Ma continental flood basalts? *Geol. Soc. Am. Bull.* 120 (11), 1478–1492.
- Wang, X.C., Li, X.H., Li, W.X., Li, Z.X., 2009. Variable involvements of mantle plumes in the genesis of mid-Neoproterozoic basaltic rocks in South China: a review. *Gondwana Res.* 15 (3–4), 381–395.
- Wang, X.C., Li, X.H., Li, Z.X., Liu, Y., Yang, Y.H., 2010. The Willouran basic province of South Australia: its relation to the Guibei large igneous province in South China and the breakup of Rodinia. *Lithos* 119 (3), 569–584.
- Wang, X.C., Li, Z.X., Li, X.H., Li, Q.L., Tang, G.Q., Zhang, Q.R., Liu, Y., 2011. Nonglacial origin for low-¹⁸O Neoproterozoic magmas in the South China Block: evidence from new *in-situ* oxygen isotope analyses using SIMS. *Geology* 39, 735–738.
- Wang, X.C., Li, X.H., Li, Z.X., Li, Q.L., Tang, G.Q., Gao, Y.Y., Zhang, Q.R., Liu, Y., 2012a. Episodic Precambrian crust growth: Evidence from U-Pb ages and Hf-O isotopes of zircon in the Nanhua Basin, central South China. *Precambr. Res.* 222–223, 386–403.
- Wang, W., Zhou, M.F., Yan, D.P., Li, J.W., 2012b. Depositional age, provenance, and tectonic setting of the Neoproterozoic Sibao Group, southeastern Yangtze Block, South China. *Precambr. Res.* 192–195, 107–124.
- Wang, X.L., Zhou, J.C., Wan, Y.S., Kitajima, K., Wang, D., Bonamici, C., Qiu, J.S., Sun, T., 2013. Magmatic evolution and crustal recycling for Neoproterozoic strongly peraluminous granitoids from southern China: Hf and O isotopes in zircon. *Earth Planet. Sci. Lett.* 366, 71–82.
- Wang, X.L., Zhou, J.C., Griffin, W.L., Zhao, G.C., Yu, J.H., Qiu, J.S., Zhang, Y.J., Xing, G.F., 2014. Geochemical zonation across a Neoproterozoic orogenic belt: isotopic evidence from granitoids and metasedimentary rocks of the Jiangnan orogen, China. *Precambr. Res.* 242, 154–171.
- Watson, E.B., Harrison, T.M., 1983. Zircon saturation revisited: temperature and composition effects in a variety of crustal magma types. *Earth Planet. Sci. Lett.* 64, 295–304.
- Weinberg, R.F., Hasalová, P., 2015. Water-fluxed melting of the continental crust: a review. *Lithos* 212–215, 158–188.
- Whalen, J.B., Currie, K.L., Chappell, B.W., 1987. A-type granites: geochemical characteristics, discrimination and petrogenesis. *Contrib. Mineral. Petro.* 95, 407–419.
- White, A.J.R., Clemens, J.D., Holloway, J.R., Silver, L.T., Chappell, B.W., Vall, V.J., 1986. S-type granites and their probable absence in southwestern North America. *Geology* 14, 115–118.
- Wu, F.Y., Jahn, B.M., Wilde, S.A., Lo, C.H., Yui, T.F., Lin, Q., Ge, W.C., Sun, D.Y., 2003. Highly fractionated I-type granites in NE China (I): geochronology and petrogenesis. *Lithos* 66, 241–273.
- Wu, R.X., Zheng, Y.F., Wu, Y.B., Zhao, Z.F., Zhang, S.B., Liu, X.M., Wu, F.Y., 2006. Reworking of juvenile crust: element and isotope evidence from Neoproterozoic granodiorite in South China. *Precambr. Res.* 146, 179–212.
- Wu, T., Xiao, L., Ma, C.Q., Pirajno, F., Sun, Y., Zhan, Q.Y., 2014a. A mafic intrusion of “arc affinity” in a post-orogenic extensional setting: a case study from Ganluogou gabbro in the northern Yidun Arc Belt, eastern Tibetan Plateau. *J. Asian Earth Sci.* 94, 139–156.
- Wu, T., Xiao, L., Gao, R., Yang, H.J., Yang, G., 2014b. Petrogenesis and tectonic setting of the Queershan composite pluton, eastern Tibetan Plateau: constraints from geochronology, geochemistry and Hf isotope data. *Sci. China, Ser. D Earth Sci.* 57, 2712–2725.
- Wu, T., Xiao, L., Wilde, S.A., Ma, C.Q., Li, Z.L., Sun, Y., Zhan, Q.Y., 2016. Zircon U-Pb age and Sr-Nd-Hf isotope geochemistry of the Ganluogou dioritic complex in the northern Triassic Yidun arc belt, Eastern Tibetan Plateau: Implications for the closure of the Garzê-Litang Ocean. *Lithos* 248–251, 94–108.
- Wu, F.Y., Liu, X.C., Ji, W.Q., Wang, J.M., Yang, L., 2017a. Highly fractionated granites: recognition and research. *Sci. China Earth Sci.* <http://dx.doi.org/10.1007/s11430-016-5139-1>.
- Wu, T., Xiao, L., Wilde, S.A., Ma, C.Q., Zhou, J.X., 2017b. A mixed source for the Late Triassic Garzê-Daocheng granitic belt and its implications for the tectonic evolution of the Yidun arc belt, eastern Tibetan Plateau. *Lithos* 288–289, 214–230.
- Xing, G.F., Wang, X.L., Wan, Y.S., Chen, Z.H., Jiang, Y., Kitajima, K., Ushikubo, T., Gopon, P., 2014. Diversity in early crustal evolution: 4100 Ma zircons in the Cathaysia Block of southern China. *Sci. Rep.* 4, 5143.
- Xu, Y., Yang, K.G., Polat, A., Yang, Z.N., 2016. The ~860 Ma mafic dikes and granitoids from the northern margin of the Yangtze Block, China: a record of oceanic subduction in the early Neoproterozoic. *Precambr. Res.* 275, 310–331.
- Yang, C., Li, X.H., Wang, X.C., Lan, Z.W., 2015. Mid-Neoproterozoic angular unconformity in the Yangtze Block revisited: insights from detrital zircon U-Pb age and Hf-O isotopes. *Precambr. Res.* 2015, 165–178.
- Yao, J.L., Shu, L.S., Santosh, M., Zhao, G.C., 2014. Neoproterozoic arc-related mafic-ultramafic rocks and syn-collision granite from the western segment of the Jiangnan Orogen, South China: constraints on the Neoproterozoic assembly of the Yangtze and Cathaysia Blocks. *Precambr. Res.* 243, 39–62.
- Yu, J.H., Wang, L.J., Griffin, W.L., O'Reilly, S.Y., Zhang, M., Li, C.Z., Shu, L.S., 2009. A Paleoproterozoic orogeny recorded in a long-lived cratonic remnant (Wuyishan terrane), eastern Cathaysia Block, China. *Precambr. Res.* 174, 347–363.
- Yu, J.H., O'Reilly, S.Y., Wang, L.J., Griffin, W.L., Zhou, M.F., Zhang, M., Shu, L.S., 2010. Components and episodic growth of Precambrian crust in the Cathaysia Block, South China: evidence from U-Pb ages and Hf isotopes of zircons in Neoproterozoic sediments. *Precambr. Res.* 181, 97–114.
- Zen, E.A., 1988. Phase relations of peraluminous granitic rocks and their petrogenetic

- implications. *Ann. Rev. Earth Planet. Sci.* 16, 21–51.
- Zhang, Y.Z., Wang, Y.J., Geng, H.Y., Zhang, Y.H., Fan, W.M., Zhong, H., 2013. Neoproterozoic (ca. 850 Ma) back-arc basin in the Central Jiangnan Orogen (Eastern South China): geochronological and petrogenetic constraints from meta-basalts. *Precambr. Res.* 231, 325–342.
- Zhao, G.C., 2015. Jiangnan Orogen in South China: developing from divergent double subduction. *Gondwana Res.* 27, 1173–1180.
- Zhao, G.C., Cawood, P.A., 1999. Tectonothermal evolution of the Mayuan assemblage in the Cathaysia Block: implications for Neoproterozoic collision-related assembly of the South China craton. *Am. J. Sci.* 299, 309–339.
- Zhao, J.H., Zhou, M.F., Yan, D.P., Zheng, J.P., Li, J.W., 2011. Reappraisal of the ages of Neoproterozoic strata in South China: no connection with the Grenvillian orogeny. *Geology* 39, 299–302.
- Zhao, J.H., Zhou, M.F., Zheng, J.P., 2013a. Constraints from zircon U-Pb ages, O and Hf isotopic compositions on the origin of Neoproterozoic peraluminous granitoids from the Jiangnan Fold Belt, South China. *Contrib. Mineral. Petrol.* 166, 1505–1519.
- Zhao, J.H., Zhou, M.F., Zheng, J.P., 2013b. Neoproterozoic high-K granites produced by melting of newly formed mafic crust in the Huangling region, South China. *Precambr. Res.* 233, 93–107.
- Zhao, Z.F., Gao, P., Zheng, Y.F., 2015. The source of Mesozoic granitoids in South China: integrated geochemical constraints from the Taoshan batholith in the Nanling Range. *Chem. Geol.* 395, 11–26.
- Zhao, K., Xu, X.S., Erdmann, S., 2017. Crystallization conditions of peraluminous charnockites: constraints from mineral thermometry and thermodynamic modeling. *Contrib. Mineral. Petrol.* 172, 26.
- Zheng, J.P., Griffin, W.L., O'Reilly, S.Y., Zhang, M., Pearson, N., Pan, Y.M., 2006. Widespread Archean basement beneath the Yangtze craton. *Geology* 34, 417–420.
- Zheng, Y.F., Zhang, S.B., Zhao, Z.F., Wu, Y.B., Li, X.H., Li, Z.X., Wu, F.Y., 2007. Contrasting zircon Hf and O isotopes in the two episodes of Neoproterozoic granitoids in South China: implications for growth and reworking of continental crust. *Lithos* 96, 127–150.
- Zhou, M.F., Yan, D.P., Kennedy, A.K., Li, Y., Ding, J., 2002. SHRIMP U-Pb zircon geochronological and geochemical evidence for Neoproterozoic arc-magmatism along the western margin of the Yangtze Block, South China. *Earth Planet. Sci. Lett.* 196, 51–67.
- Zhou, J.C., Wang, X.L., Qiu, J.S., 2009. Geochronology of Neoproterozoic mafic rocks and sandstones from northeastern Guizhou, South China: coeval arc magmatism and sedimentation. *Gondwana Res.* 170, 27–42.